Cell Metabolism
Article

Regulation of Hepatic Energy Metabolism and Gluconeogenesis by BAD

Alfredo Giménez-Cassina,[1,2,7] Luisa Garcia-Haro,[1,2,7] Cheol Soo Choi,[3,4,7] Mayowa A. Osundiji,[1,2] Elizabeth A. Lane,[1,2] Hu Huang,[5] Muhammed A. Yildirim,[1] Benjamin Szlyk,[1] Jill K. Fisher,[1] Klaudia Polak,[1] Elaura Patton,[1] Jessica Wiwczar,[1] Marina Godes,[1] Dae Ho Lee,[5] Kirsten Robertson,[1] Sheene Kim,[3] Ameya Kulkarni,[3] Alberto Distefano,[3] Varman Samuel,[3] Gary Cline,[3] Young-Bum Kim,[5] Gerald I. Shulman,[3,6] and Nika N. Danial[1,2,*]
[1]Department of Cancer Biology, Dana-Farber Cancer Institute, Boston, MA 02215, USA
[2]Department of Cell Biology, Harvard Medical School, Boston, MA 02115, USA
[3]Department of Internal Medicine, Yale University School of Medicine, New Haven, CT 06510, USA
[4]Division of Endocrinology, Lee Gil Ya Cancer and Diabetes Institute, Gil Medical Center, Gachon University, Incheon 405-760, Korea
[5]Division of Endocrinology, Diabetes and Metabolism, Department of Medicine, Beth Israel Deaconess Medical Center and Harvard Medical School, Boston, MA 02115, USA
[6]Howard Hughes Medical Institute, Yale University School of Medicine, New Haven, CT 06510, USA
[7]These authors contributed equally to this work
*Correspondence: nika_danial@dfci.harvard.edu
http://dx.doi.org/10.1016/j.cmet.2013.12.001

SUMMARY

The homeostatic balance of hepatic glucose utilization, storage, and production is exquisitely controlled by hormonal signals and hepatic carbon metabolism during fed and fasted states. How the liver senses extracellular glucose to cue glucose utilization versus production is not fully understood. We show that the physiologic balance of hepatic glycolysis and gluconeogenesis is regulated by Bcl-2-associated agonist of cell death (BAD), a protein with roles in apoptosis and metabolism. BAD deficiency reprograms hepatic substrate and energy metabolism toward diminished glycolysis, excess fatty acid oxidation, and exaggerated glucose production that escapes suppression by insulin. Genetic and biochemical evidence suggests that BAD's suppression of gluconeogenesis is actuated by phosphorylation of its BCL-2 homology (BH)-3 domain and subsequent activation of glucokinase. The physiologic relevance of these findings is evident from the ability of a BAD phosphomimic variant to counteract unrestrained gluconeogenesis and improve glycemia in leptin-resistant and high-fat diet models of diabetes and insulin resistance.

INTRODUCTION

Hepatic glucose production (HGP) is central to metabolic adaptation during fasting, and its abnormal elevation is a chief determinant of fasting hyperglycemia in diabetes (Lin and Accili, 2011; Rizza, 2010). During short-term fasting, glucose is produced by both net glycogenolysis and gluconeogenesis (Rothman et al., 1991), whereas upon prolonged fasting, glucose is synthesized almost exclusively from gluconeogenesis. Gluconeogenesis and glycolysis are competing pathways that are reciprocally regulated by glucagon and insulin during fasted and fed states, respectively. In addition to transcriptional regulation, changes in hepatic carbon flux can exert allosteric effects on gluconeogenic enzymes (Magnuson et al., 2003). Hepatic substrate flux is further intertwined with fatty acid oxidation (FAO), tricarboxylic acid (TCA) cycle, and mitochondrial electron transport chain activity, which supply the gluconeogenic pathway with carbon substrates, reducing equivalents, and ATP (Satapati et al., 2012).

We have previously shown that the BCL-2 family protein Bcl-2-associated agonist of cell death (BAD) has an alternative function in glucose metabolism, separate from its role in apoptosis (Danial, 2008; Danial et al., 2003; Danial et al., 2008). BAD's metabolic effect is dependent on its ability to activate glucokinase (GK) and modulate glucose oxidation (Danial, 2008; Danial et al., 2008). GK is the product of the maturity-onset diabetes of the young type 2 (*MODY2*) gene that exerts tissue-restricted functions (Matschinsky, 2009). In liver, GK regulates substrate utilization and storage by stimulating glycogen and lipid synthesis while suppressing hepatic glucose production (Postic et al., 1999; Rossetti et al., 1997; Velho et al., 1996). In β cells, GK is critical for glucose regulation of insulin secretion (Matschinsky, 2009). We previously reported that in β cells, GK activation and glucose sensing are attuned to BAD phosphorylation on S155 within an amphipathic α-helical region known as the BCL-2 homology (BH)-3 domain. BAD S155 is the target of multiple kinases that either phosphorylate S155 directly or modify upstream priming phosphorylation sites, facilitating S155 phosphorylation (reviewed in Danial, 2008). Phosphorylation of the BH3 domain not only triggers BAD's metabolic function, but also suppresses its apoptotic activity. Importantly, the phospho-BAD BH3 helix is both required and sufficient for BAD's metabolic function (Danial et al., 2008). Recent biochemical and structural dissection of the BAD-GK complex has revealed that the phospho-BAD BH3 helix directly engages GK near its active site and increases the V_{max} of the enzyme without drastic effects on its glucose affinity (Szlyk et al., 2014).

Beyond β cell abnormalities, the contribution of altered hepatic metabolism to glucose homeostasis defects associated with loss of BAD has not been examined. This is especially

relevant as the regulatory networks that modulate GK activity in liver are distinct from β cells (Matschinsky, 2009). Here, we use a combination of informative genetic models and BAD mutants to investigate the significance of BAD and its partnership with GK in hepatic substrate utilization and glucose production. Moreover, we probe the physiologic relevance of hepatic BAD in restoring proper control of glucose production in the leptin-resistant and high-fat diet models of diabetes and insulin resistance.

RESULTS

BAD-Dependent Modulation of Hepatic Glucose Metabolism

To define the contribution of altered hepatic metabolism to glucose homeostasis abnormalities in *Bad*$^{-/-}$ mice, we initially focused on glycolytic and gluconeogenic pathways. In primary *Bad*$^{-/-}$ hepatocytes, lactate production in response to glucose was diminished (Figure 1A), and gluconeogenesis was significantly exaggerated, as apparent from glucose release in response to lactate and pyruvate (Figure 1B). These observations suggest that the net balance of glycolysis and gluconeogenesis is shifted toward gluconeogenesis in the absence of BAD. Pyruvate tolerance tests (PTTs) confirmed that *Bad*$^{-/-}$ mice display significantly higher gluconeogenic conversion of pyruvate to glucose in vivo (Figure 1C). Importantly, knockdown of *Bad* in primary wild-type hepatocytes was sufficient to reduce glycolysis and enhance gluconeogenesis (Figures 1D and 1E), indicating an acute and cell-autonomous role for BAD in these processes.

Impaired PTT in *Bad*$^{-/-}$ mice is consistent with changes in hepatic glucose metabolism. However, secondary changes due to chronic whole-body deletion of *Bad* cannot be excluded. To directly examine the relevance of hepatic BAD in vivo, *Bad* was knocked down in the liver of C57BL/6J mice following tail vein delivery of adenoviruses bearing *Bad* shRNA or control (scrambled) sequence (Figure S1A available online). Hepatic depletion of BAD manifested in excess glucose production during PTT and fasting hyperglycemia (Figure 1F). In addition, acute hepatic knockdown of *Bad* resulted in impaired glucose tolerance (Figure S1B), similar to *Bad*$^{-/-}$ mice (Danial et al., 2003). Notably, hepatic depletion of BAD did not alter insulin secretion in response to a glucose challenge in vivo (Figure S1C). In addition, fed and fasted insulin levels were comparable in mice treated with *Bad* shRNA versus control shRNA (Figure S1D). Collectively, the above in vitro and in vivo observations indicate that hepatic BAD influences the fate of pyruvate and is relevant for the proper regulation of glucose utilization and production in the liver.

Hepatic pyruvate metabolism is regulated, at least in part, at the transcriptional level downstream of hormonal and nutrient signaling (Lin and Accili, 2011). Initial examination of gluconeogenic and glycolytic genes in fed and fasted *Bad*$^{-/-}$ and *Bad* knockdown liver indicated changes in several genes. In particular, mRNA levels of the gluconeogenic enzyme phosphoenolpyruvate carboxykinase (*Pck*) 1 were significantly elevated, while mRNA levels of the glycolytic enzyme liver-type pyruvate kinase (*L-Pk*) were significantly diminished (Figures 1G, 1H, and S1E). Other gluconeogenic genes (fructose 1,6-bisphosphatase [*Fbp*] 1 and glucose 6-phosphatase [*G6Pase*]) were also increased in *Bad*$^{-/-}$ liver (Figure S1E). This is further consistent with BAD-dependent reciprocal changes in hepatic glycolysis and gluconeogenesis.

In addition to transcriptional control during fed and fasted states, *L-Pk* and *Pck1* expression can be regulated by glucose. Specifically, the promoters of both genes are glucose sensitive in that increased glucose metabolism through GK stimulates *L-Pk* transcription and represses that of *Pck1* (Cournarie et al., 1999; Scott et al., 1998; Yamada and Noguchi, 1999). Based on these reports, we predicted that glucose modulation of *L-Pk* and *Pck1* transcription may be altered upon hepatic depletion of BAD and the attendant diminution of glucose metabolism. This was indeed the case. In wild-type hepatocytes, *L-Pk* mRNA levels were elevated at high, compared to low, glucose concentrations (25 mM versus 5 mM), whereas *Pck1* mRNA levels showed the opposite profile (Figures S1F and S1G). *Bad* knockdown, however, resulted in higher *Pck1* mRNA levels that were especially exaggerated at low glucose (Figure S1F). In comparison, glucose stimulation of *L-Pk* transcripts was significantly reduced (Figure S1G).

The above observations in both cultured hepatocytes and whole animals using a combination of biochemical and transcriptional readouts suggest that BAD is required for proper interpretation of glucose signals. Notably, the metabolic outcome of BAD depletion in the liver was phenocopied in mice treated with *Gk* shRNA (Figure S1H). This is evident from exaggerated glucose levels during PTT, significant elevation of hepatic *Pck1* mRNA levels, and diminution of *L-Pk* transcripts, as well as impaired glucose tolerance (Figures 1I–1K and S1I). Given the biochemical interaction between BAD and GK (Danial et al., 2003, 2008; Szlyk et al., 2014), these shared metabolic outcomes suggest that their functional partnership may be relevant for the proper control of glycolysis and gluconeogenesis in the liver (see below).

We have previously reported that BAD's capacity to activate GK in β cells is triggered by S155 phosphorylation (aa enumeration based on the mouse sequence of BAD) (Danial et al., 2008). Importantly, S155 phosphorylation is sensitive to nutrient status in both β cells (Danial et al., 2008) and liver (Figure 2A). Specifically, BAD S155 phosphorylation is induced upon refeeding. In addition, the phosphorylation of two priming serine residues upstream of the BAD BH3 domain, S112 and S136, is similarly increased upon refeeding (Figure 2A). These observations suggest that BAD phosphorylation and metabolic activity may be integrated with nutritional states. Consistent with this idea, interference with BAD phosphorylation through a *Bad* S155A nonphosphorylatable knockin allele was associated with fasting hyperglycemia and excess glucose release during PTT (Figure 2B).

To interrogate the direct significance of BAD phosphorylation specifically in the liver, we carried out whole animal liver reconstitution assays in *Bad*$^{-/-}$ mice using adenoviruses expressing wild-type or defined phosphorylation mutants within the BAD BH3 domain. Hepatic reconstitution with wild-type BAD lowered the glucose values during PTT, indicating that exaggerated gluconeogenesis in *Bad*$^{-/-}$ is directly related to the loss of BAD function in the liver (Figure 2C). Given BAD's dual capacity to engage GK and influence glucose metabolism on one hand, and to bind select BCL-2 protein (BCL-2, BCL-X_L, and BCL-w)

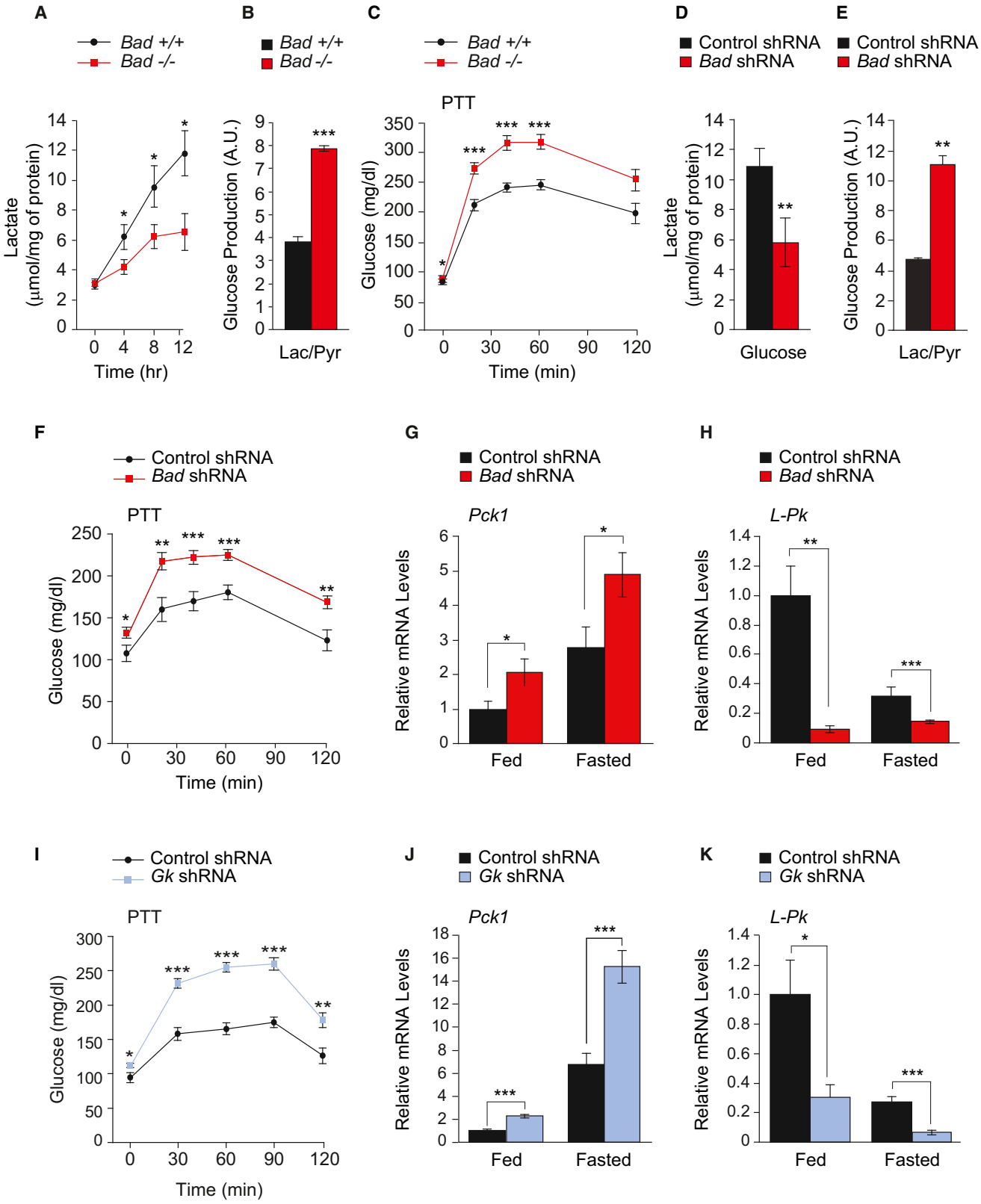

Figure 1. Hepatic Glucose Metabolism in the Absence of BAD

(A) Glucose-stimulated lactate production by primary $Bad^{+/+}$ and $Bad^{-/-}$ hepatocytes (n = 5–8).

(B) Glucose release by $Bad^{+/+}$ and $Bad^{-/-}$ hepatocytes treated with lactate and pyruvate (n = 6).

(legend continued on next page)

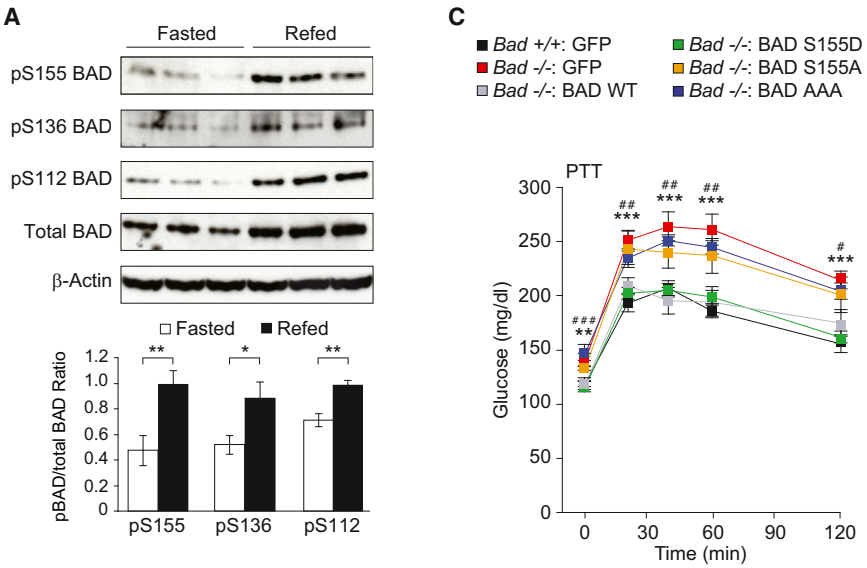

Figure 2. The Effect of BAD Phosphorylation on Gluconeogenesis

(A) Immunoblot analysis and quantification of relative BAD phosphorylation on S155, S136, and S112 in liver samples derived from C57BL/6J mice fasted overnight and refed for 6 hr after overnight fasting.

(B) PTT in $Bad^{+/+}$ and S155A knockin mice (n = 10–11).

(C) PTT in $Bad^{+/+}$ and $Bad^{-/-}$ mice following hepatic reconstitution with the indicated adenoviruses (n = 16–24). Asterisks compare $Bad^{-/-}$:BAD S155D versus $Bad^{-/-}$:GFP; # indicates a comparison of $Bad^{-/-}$:BAD WT versus $Bad^{-/-}$:GFP.

(D) Glucose production in primary $Bad^{-/-}$ hepatocytes reconstituted with the indicated adenoviruses and treated with lactate and pyruvate (n = 7–12). Error bars show ± SEM. *p < 0.05; **p < 0.01; ***p < 0.001; n.s., nonsignificant. See also Figure S2.

and influence the sensitivity of cells to apoptosis on the other, a definitive role for BAD's metabolic function in regulation of gluconeogenesis could not be inferred solely based on the phenotype of wild-type BAD in these assays. Therefore, we examined three separate BAD phosphorylation mutants that are competent or deficient in activating GK (Figure S2A). The phosphomimic S155D mutation triggers BAD's capacity to activate GK while blocking its interaction with BCL-2 protein partners (Danial et al., 2008). Hepatic reconstitution with this mutant was sufficient to restore GK activity and correct the PTT profile of $Bad^{-/-}$ mice (Figures 2C and S2B). The corresponding phospho-deficient variant, BAD S155A, which is compromised in its capacity to restore hepatic GK activity in $Bad^{-/-}$ mice (Figure S2B), did not correct the glucose values during PTT (Figure 2C). Although diminished in its ability to activate GK, BAD S155A retains its capacity to interact with BCL-2 family partners (Danial, 2008) and is therefore not a direct control for S155D GK-activating variant, which does not bind to BCL-2 family proteins (Figure S2A). For these reasons, we used a second phospho-deficient BAD variant that has diminished GK-activating capacity but cannot bind BCL-2 family partners (BAD L151A, S155A, and D156A triple mutant referred to as BAD AAA) (Figures S2A and S2B) (Danial et al., 2008). Parallel comparison of this mutant with BAD S155D allowed assessment of BAD's capacity to engage and activate GK separate from its ability to bind BCL-2 family partners. Unlike BAD S155D, BAD AAA did not restore the PTT profile in $Bad^{-/-}$ mice (Figure 2C). Furthermore, in vitro genetic reconstitution studies using these variants were consistent with the above observations in that BAD S155D, but not BAD

(C) PTT in $Bad^{+/+}$ and $Bad^{-/-}$ mice (n = 14–20).
(D) Lactate production in *Bad* knockdown hepatocytes 8 hr after glucose stimulation (n = 9).
(E) Glucose production in *Bad* knockdown hepatocytes treated with lactate and pyruvate (n = 3–5).
(F) PTT in C57BL/6J mice after hepatic knockdown of *Bad* (n = 12–17).
(G and H) Relative hepatic mRNA levels of *Pck1* (G) and *L-Pk* (H) in fed and overnight-fasted C57BL/6J mice after hepatic knockdown of *Bad* (n = 10).
(I) PTT in C57BL/6J mice after hepatic knockdown of *Gk* (n = 8–12).
(J and K) Relative hepatic mRNA levels of *Pck1* (J) and *L-Pk* (K) in fed and overnight-fasted C57BL/6J mice after hepatic knockdown of *Gk* (n = 5). Error bars show ± SEM. *p < 0.05; **p < 0.01; ***p < 0.001. See also Figure S1.

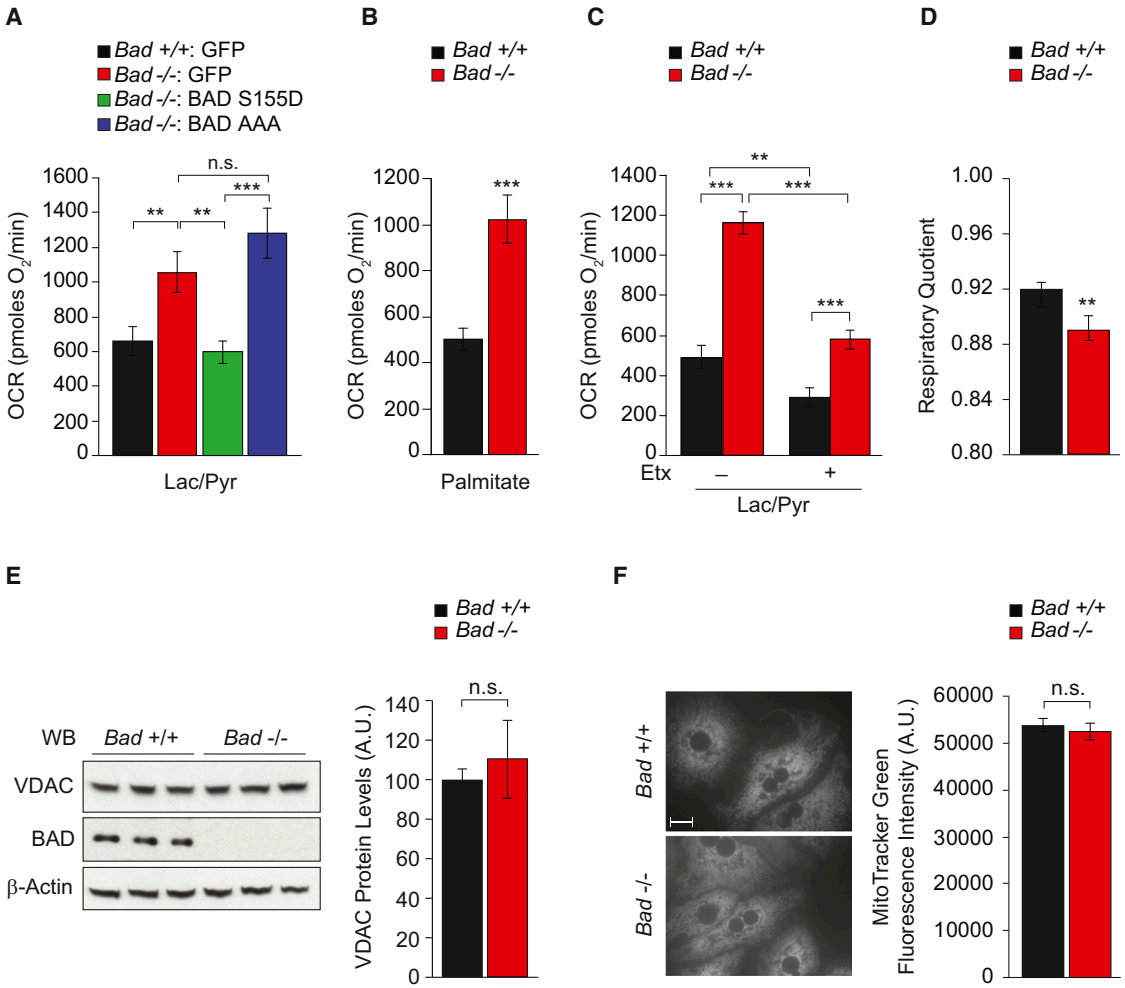

Figure 3. BAD-Dependent Modulation of Hepatic Energy Metabolism

(A) Mitochondrial OCR in primary $Bad^{+/+}$ and $Bad^{-/-}$ hepatocytes transduced with the indicated adenoviruses and treated with lactate and pyruvate (n = 4).

(B) Mitochondrial OCR in primary $Bad^{+/+}$ and $Bad^{-/-}$ hepatocytes treated with palmitate (n = 10).

(C) Etomoxir (Etx) inhibition of OCR in primary hepatocytes treated with lactate and pyruvate (n = 5).

(D) Respiratory quotient in $Bad^{+/+}$ and $Bad^{-/-}$ mice (n = 8).

(E and F) Comparison of mitochondrial mass as examined by the protein levels of Voltage-dependent anion channel (VDAC) using western blot analysis (E) and by the fluorescence signal intensity of MitoTracker Green in $Bad^{+/+}$ and $Bad^{-/-}$ primary hepatocytes (F) (n = 3). Scale bar in (F), 10 μm. Error bars show ± SEM. **p < 0.01; ***p < 0.001; n.s., nonsignificant. See also Figure S3 and Table S1.

S155A or BAD AAA, corrected gluconeogenesis in $Bad^{-/-}$ hepatocytes to levels comparable to those of GFP-expressing $Bad^{+/+}$ controls (Figure 2D). Thus, in vivo and in vitro interference with BAD S155 phosphorylation is associated with unrestrained gluconeogenesis and phenocopies the changes in hepatic metabolism observed in $Bad^{-/-}$ and *Bad* knockdown liver.

BAD's Effect on Mitochondrial Energy Metabolism in Hepatocytes

Mitochondria play a pivotal role in gluconeogenesis through provision of carbon substrates, reducing equivalents, and ATP (Burgess et al., 2007; Satapati et al., 2012). Metabolic flux analysis has also uncovered a tight connection between PCK1, mitochondrial bioenergetics, and TCA cycle (Burgess et al., 2007; Hakimi et al., 2005; Satapati et al., 2012). To assess how $Bad^{-/-}$ hepatocytes derive the ATP required to support excess gluconeogenesis, we focused on mitochondrial energy metabolism. We reasoned that gluconeogenesis from exogenous lactate and pyruvate would create a state of energy demand, driving ATP production by mitochondrial oxidative phosphorylation, which can be deduced from the fraction of mitochondrial oxygen consumption rate (OCR) that is sensitive to the mitochondrial ATP synthase inhibitor oligomycin. In the presence of lactate and pyruvate, $Bad^{-/-}$ hepatocytes showed a significantly higher induction of mitochondrial ATP production (Figure 3A and Table S1), which was restored to wild-type values after genetic introduction of the BAD S155D variant, but not the BAD AAA mutant (Figure 3A and Table S1).

Gluconeogenesis and mitochondrial FAO are interdependent. For example, fatty acids augment flux through pyruvate

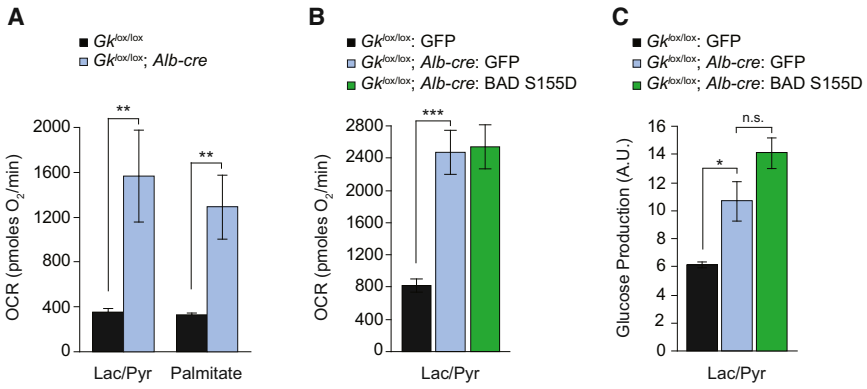

Figure 4. Hepatic Function of BAD Is GK Dependent

(A) Mitochondrial OCR in GK-deficient hepatocytes treated with lactate and pyruvate or palmitate (n = 8–10).

(B and C) Shown is mitochondrial OCR (B) and glucose production (C) in GK-deficient hepatocytes transduced with the indicated adenoviruses (n = 9). Error bars show ± SEM. *p < 0.05; **p < 0.01; ***p < 0.001; n.s., nonsignificant. See also Table S1.

carboxylase, leading to significant stimulation of OCR and gluconeogenesis in the presence of lactate and pyruvate (Gustafson et al., 2001; Pryor et al., 1987). Importantly, inhibition of carnitine palmitoyl transferase (CPT1), which is required for mitochondrial import of long-chain fatty acids, or interference with mitochondrial electron transport chain activity reverses these effects (Pryor et al., 1987), indicating the importance of mitochondria in energetic and substrate coupling between FAO and gluconeogenesis. This prompted examination as to whether increased gluconeogenesis in the absence of BAD is linked to elevated FAO. Indeed, mitochondrial OCR in response to palmitate was significantly higher in primary *Bad*$^{-/-}$ hepatocytes compared with controls (Figure 3B and Table S1). Similar results were also obtained in *Bad* knockdown hepatocytes (data not shown). As predicted, the rise in OCR normally seen upon treatment with lactate and pyruvate was inhibited by the mitochondrial FAO inhibitor etomoxir (Etx) in both *Bad*$^{+/+}$ and *Bad*$^{-/-}$ hepatocytes (Figure 3C). However, the etomoxir-inhibitable portion of this respiratory rate was significantly larger in *Bad*$^{-/-}$ than in control hepatocytes (Figure 3C and Table S1), which is in agreement with higher FAO in *Bad*$^{-/-}$ hepatocytes (Figure 3B). This is also consistent with a lower respiratory quotient (RQ) in *Bad*$^{-/-}$ mice (Figure 3D), which reflects preferential utilization of fatty acids as energy source. Overall, these results suggest that loss of BAD is associated with an altered program of mitochondrial substrate and energy metabolism that matches excess gluconeogenesis. Notably, these alterations do not appear to be linked to changes in mitochondrial mass in the absence of BAD (Figures 3E and 3F).

The functional increase in FAO in the absence of BAD warranted examination of hepatic genes involved in fatty acid metabolism. Comparison of microarray expression profiles using gene set enrichment analysis (GSEA) identified the mitochondrial β-oxidation pathway as the top gene set enriched in fasted *Bad*$^{-/-}$ liver compared to *Bad*$^{+/+}$ controls (Figure S3A). Quantitative real-time PCR provided independent evidence for augmented mRNA abundance of the FAO genes in *Bad*$^{-/-}$ liver (Figure S3B). Conversely, transcription of the lipogenic gene acetyl coenzyme A (acetyl-CoA) carboxylase (*Acc*) was markedly downregulated in *Bad*$^{-/-}$ liver (Figure S3B). Examination of key transcriptional regulators of FAO also indicated significant induction of *Pparα* mRNA in *Bad*$^{-/-}$ liver (Figure S3B). Importantly, these transcriptional changes were also observed following acute hepatic knockdown of *Bad* (Figure S3C) and were further phenocopied by acute hepatic knockdown of *Gk* (Figure S3D) or liver-specific deletion of *Gk* (*Gk*$^{lox/lox}$ versus *Gk*$^{lox/lox}$; *Alb-cre*; Figure S3E). These observations suggest a potential link between BAD- and GK-dependent metabolic signaling and hepatic gene expression.

Hepatic Function of BAD Is Mediated by GK

The differential effect of BAD S155D and AAA variants in genetic reconstitution assays suggests that BAD's influence on glycolysis and gluconeogenesis is coordinated with its ability to activate GK. In addition, the common phenotype of exaggerated gluconeogenesis and FAO when either BAD or GK are acutely depleted in the liver suggests that the functional interaction of these two proteins is relevant for hepatic substrate metabolism. This predicts that loss of GK would phenocopy loss of BAD in mitochondrial energy metabolism and handling of gluconeogenic substrates and that BAD's effect on hepatic substrate utilization would be abrogated in the genetic background of *Gk* deficiency. We next tested each of these predictions. Primary *Gk*$^{-/-}$ hepatocytes display marked stimulation of mitochondrial OCR when cultured with lactate and pyruvate or palmitate (*Gk*$^{lox/lox}$ versus *Gk*$^{lox/lox}$; *Alb-cre*; Figures 4A and 4B; Table S1) analogous to *Bad*$^{-/-}$ hepatocytes. Gluconeogenesis was also significantly higher in *Gk* null hepatocytes (Figure 4C). However, expression of BAD S155D in *Gk*$^{-/-}$ hepatocytes was ineffective in curtailing excess mitochondrial OCR and glucose production in the presence of lactate and pyruvate (Figures 4B and 4C). This contrasts with the capacity of BAD S155D to correct these parameters in *Bad*$^{-/-}$ hepatocytes (Figures 2D and 3A). These data provide genetic and mechanistic evidence consistent with GK as a downstream mediator of BAD's effect on hepatic substrate and energy metabolism.

Hepatic Insulin Resistance in *Bad*$^{-/-}$ mice

Insulin is a critical regulator of hepatic glucose metabolism through transcriptional and posttranslational mechanisms as well as modulation of substrate supply (Lin and Accili, 2011; Saltiel and Kahn, 2001). It stimulates transcription of several glycolytic genes, including *Gk*, and represses that of gluconeogenic genes *Pck1*, *Fbp1*, and *G6p*. In addition, insulin stimulates BAD phosphorylation in the liver (Figure 5A). Given the effect of BAD phosphorylation on GK activity and hepatic substrate utilization, these observations predict that BAD's hepatic function may be subject to insulin regulation. To test the physiologic relevance of BAD in the context of insulin action, we performed euglycemic-hyperinsulinemic clamp analysis. While glucose

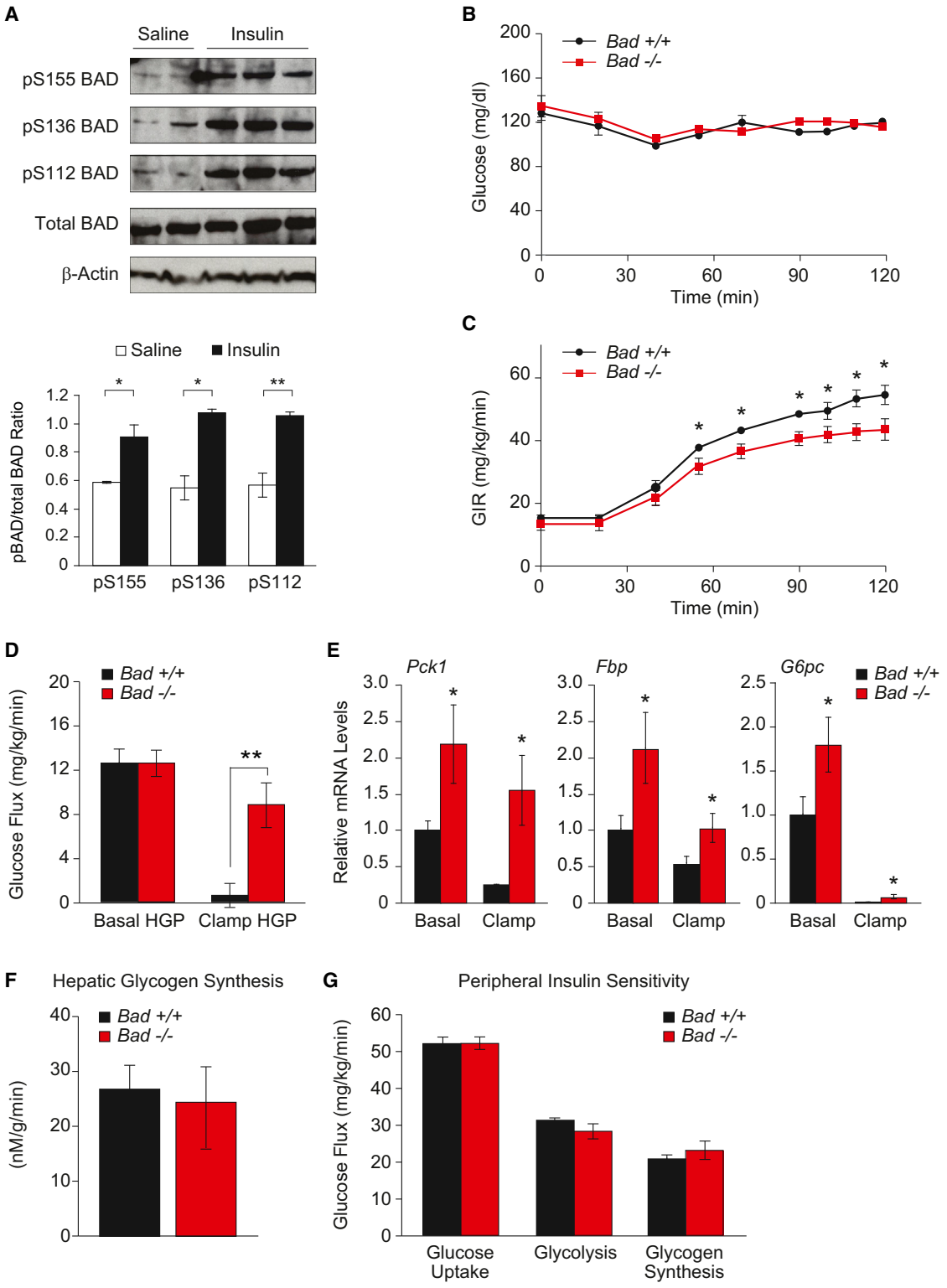

Figure 5. Hepatic Insulin Resistance in the Absence of BAD

(A) Modulation of hepatic BAD phosphorylation by insulin in vivo. Immunoblot analysis and quantification of relative BAD phosphorylation on S155, S136, and S112 in liver samples derived from C57BL/6J mice fasted overnight and injected with saline or insulin.

(B–G) Euglycemic-hyperinsulinemic clamp analysis in *Bad*$^{-/-}$ and *Bad*$^{+/+}$ mice (n = 7–9), showing plasma glucose (B), glucose infusion rate (GIR) (C), hepatic glucose production (HGP) (D), relative mRNA abundance of hepatic gluconeogenic genes (E), hepatic glycogen synthesis rates (F), and peripheral insulin sensitivity (G). Error bars show ± SEM. *p < 0.05; **p < 0.01; *Bad*$^{-/-}$ versus *Bad*$^{+/+}$ mice. See also Figure S4.

was maintained at basal concentration (~6.7 mM) throughout the analysis (Figure 5B), *Bad*$^{-/-}$ mice displayed a small, but statistically significant, reduction in glucose infusion rates (GIR) (51.5 ± 2.5 versus 43.4 ± 2.6 mg/kg/min, $p < 0.05$, *Bad*$^{+/+}$ versus *Bad*$^{-/-}$; Figure 5C), consistent with whole-body insulin resistance. As reduced GIR can derive from impaired suppression of HGP by insulin and/or its diminished capacity to enhance glucose uptake in peripheral tissues, hepatic and peripheral insulin sensitivities were measured separately. Suppression of HGP by insulin in *Bad*$^{-/-}$ mice was markedly impaired, consistent with hepatic insulin resistance (94.7% ± 14.7% versus 32.1% ± 14.0%, $p < 0.008$, *Bad*$^{+/+}$ versus *Bad*$^{-/-}$; Figure 5D). This was further consistent with diminished capacity of insulin to fully inhibit the transcription of *Pck1*, *Fbp1*, and the catalytic subunit of *G6p* (*G6pc*) in *Bad*$^{-/-}$ liver (Figure 5E).

To determine if hepatic insulin resistance in BAD-deficient mice extends to abnormalities in glucose storage, the net hepatic glycogen synthesis rates were also measured and found to be comparable in *Bad*$^{+/+}$ and *Bad*$^{-/-}$ mice (Figure 5F). These rates reflect the net balance of direct and indirect pathways of glycogen synthesis (Agius, 2008). While diminished hepatic glucose utilization in *Bad*$^{-/-}$ mice (Figure 1A) would predict lower glycogen synthesis via the direct pathway, increased gluconeogenesis in these animals may lead to a larger contribution from the indirect pathway. It is possible that a relative increase in the indirect pathway of glycogen synthesis may have offset any differences in the direct pathway, rendering total glycogen synthesis in *Bad*$^{-/-}$ mice comparable to that of controls. Notably, a prominent contribution of the gluconeogenic pathway to hepatic glycogen synthesis in glucokinase-deficient (*MODY2*) subjects has been reported (Velho et al., 1996).

Insulin resistance in *Bad*$^{-/-}$ mice is restricted to liver, as insulin-mediated glucose uptake in skeletal muscle and white adipose tissues was not altered (Figures S4A and S4B). Whole-body glucose uptake, glycolysis, and glycogen synthesis did not reveal any differences in the two genotypes (Figure 5G). Other metabolic parameters, such as fat and lean mass, energy expenditure, and activity, as well as fasted serum levels of glucagon, FFA, and triglycerides, were comparable in both genotypes (Figures S4C–S4H). Overall, these results indicate that peripheral insulin sensitivity is preserved in *Bad*$^{-/-}$ mice and that diminished GIR in this genetic model can be chiefly attributed to impaired suppression of HGP.

Hepatic Insulin Signaling in the Absence of BAD

Impaired hepatic insulin action in *Bad*$^{-/-}$ mice warranted examination of insulin signaling. Insulin stimulation of phosphatidylinositol 3-kinase (PI3K) activity was significantly diminished in *Bad*$^{-/-}$ liver, but not in *Bad*$^{-/-}$ gastrocnemius muscle (Figures 6A and S5A). Lower hepatic PI3K activity in *Bad*$^{-/-}$ was consistent with reduced stimulation of AKT phosphorylation by insulin but could not be explained by changes in insulin receptor (IR) phosphorylation (Figure 6B). Importantly, insulin stimulation of AKT phosphorylation was not altered in muscle (Figure S5B), which is in agreement with selective loss of insulin action in liver, but not in muscle (Figures 5D and S4A). Reduced AKT phosphorylation in response to insulin was further evident in primary *Bad*$^{-/-}$ hepatocytes treated with insulin (Figure S5C), indicating a cell-autonomous effect of BAD deficiency on insulin signaling. Moreover, attenuated insulin signaling in *Bad*$^{-/-}$ mice was recapitulated in mice treated with *Bad* shRNA (Figure 6C). Reduced PI3K-AKT signaling without alterations in insulin receptor phosphorylation predicts inhibition at the level of insulin receptor substrate 1 (IRS-1) through negative feedback loops (Copps and White, 2012). Examination of several IRS-1 inhibitory kinases revealed comparable hepatic c-Jun amino-terminal kinase (JNK) and extracellular signal-regulated kinase (ERK) phosphorylation but diminished glycogen synthase kinase-3 (GSK-3) phosphorylation in *Bad* shRNA liver (Figure 6C and data not shown). Because phosphorylation inactivates GSK-3, these results indicate increased hepatic GSK-3 activity in BAD-depleted liver. However, GSK-3 phosphorylation is itself regulated by insulin, similar to several other IRS-1 inhibitory kinases (Copps and White, 2012), and whether GSK-3 activity is the cause or consequence of reduced insulin signaling in these mice remains to be determined. Importantly, an analogous decline in hepatic insulin signaling was also observed in mice treated with *Gk* shRNA (Figure 6D). This is consistent with published reports that loss of GK or inhibition of its activity is associated with blunted suppression of HGP and hepatic insulin resistance (Barzilai et al., 1996; Clément et al., 1996; Rossetti et al., 1997). In aggregate, our findings indicate that, similar to hepatic depletion or inhibition of GK, loss of BAD and the attendant diminution of GK activity are associated with reduced hepatic insulin sensitivity and insulin signaling.

Hepatic GK and BAD are both regulated by insulin. *Gk* is a transcriptional target of sterol regulatory element-binding protein 1c (SREBP1c) downstream of the PI3K-AKT axis, and BAD phosphorylation, which stimulates GK activity (Figure S2B) (Szlyk et al., 2014), is induced by insulin (Figure 5A). It is therefore possible that BAD may serve as an additional downstream mediator of insulin's effect on GK, whereby insulin stimulates GK activity beyond induction of *Gk* transcription. Given insulin regulation of BAD and GK and reduced insulin signaling in *Bad*$^{-/-}$ mice, two potential scenarios may explain the diminished insulin suppression of HGP in these mice: diminished insulin stimulation of *Gk* expression or diminished capacity of insulin to enhance GK activity through BAD phosphorylation. To determine changes in *Gk* expression in this setting, we examined hepatic *Srebp1c* and *Gk* mRNA levels in *Bad*$^{+/+}$ and *Bad*$^{-/-}$ mice subjected to euglycemic-hyperinsulinemic clamp. Relative *Srebp1c* mRNA abundance was lower in *Bad*$^{-/-}$ liver (Figure S5D), which is consistent with reduced insulin stimulation of PI3K-AKT signaling in these mice. Surprisingly, however, *Gk* mRNA levels were not diminished in these samples (Figure S5E), suggesting potential SREBP1c-independent compensatory mechanisms that maintain *Gk* mRNA levels despite reduced insulin signaling in *Bad*$^{-/-}$ liver. Notably, several other transcription factors can directly activate the *Gk* promoter in the absence of SREBP1c (Bechmann et al., 2012; Kim et al., 2009; Oosterveer et al., 2012). Moreover, *Gk* mRNA levels can be regulated by 6-phosphofructo-2-kinase/fructose-2,6-bisphosphatase (PFK2) independent of insulin and SREBP1c (Payne et al., 2005; Wu et al., 2004). Therefore, it is possible that one or more of these mechanisms may stabilize *Gk* expression in *Bad*$^{-/-}$ liver under these conditions. In addition, the potential contribution of residual insulin signaling in these mice cannot be ruled out. Regardless of the mechanisms that may stabilize *Gk* mRNA

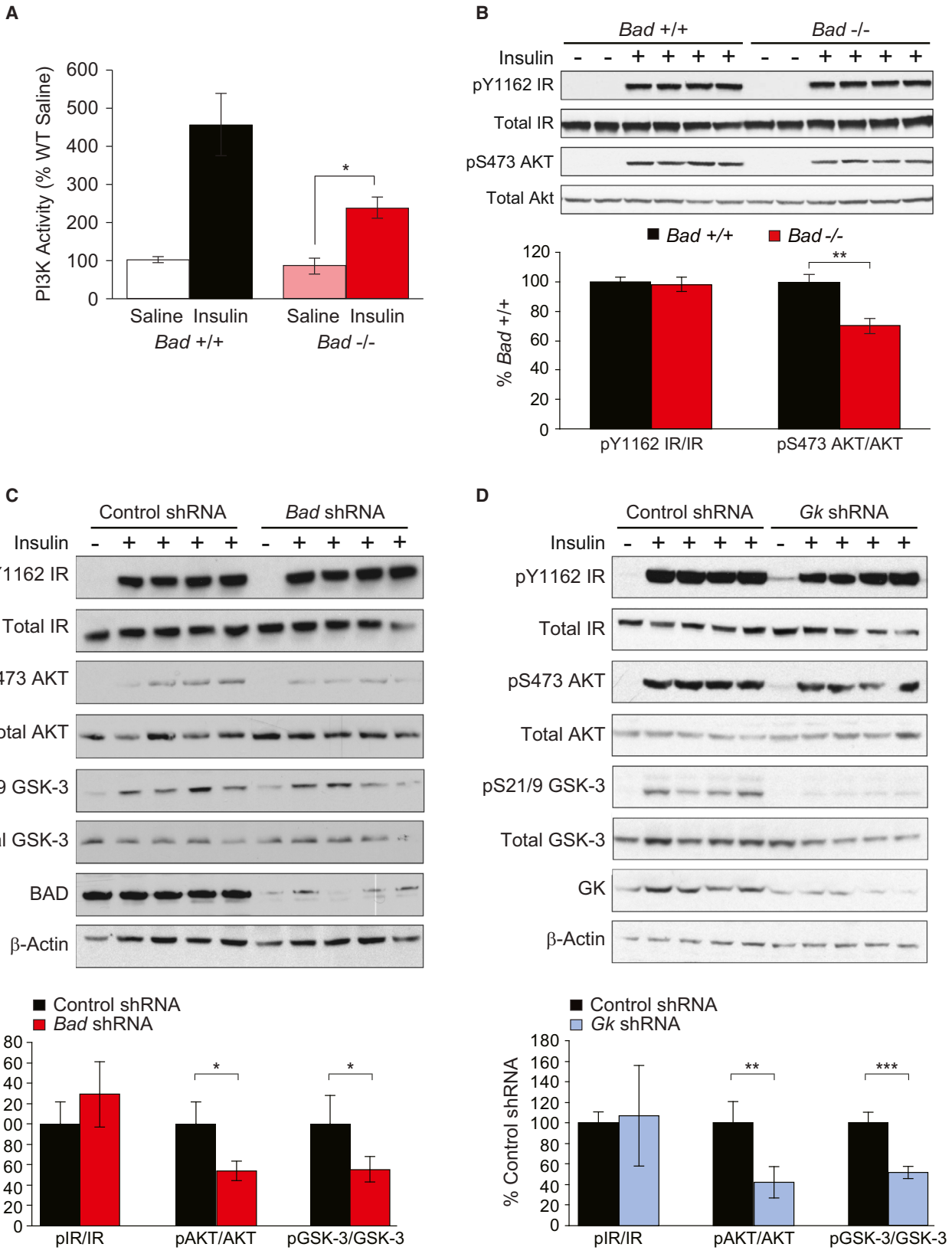

(legend on next page)

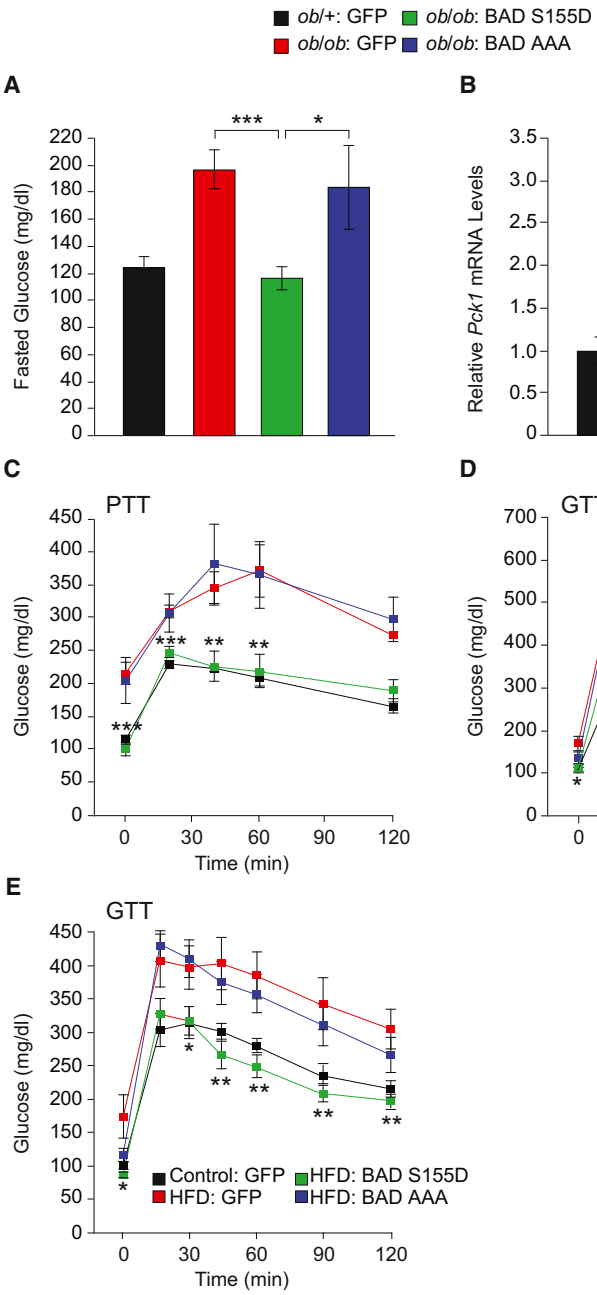

Figure 7. Metabolic Effects of BAD in *ob/ob* and HFD-Treated Mice

(A–D) Shown are fasting glucose levels (A), liver *Pck1* mRNA abundance (B), and pyruvate (C) and glucose (D) tolerance tests following hepatic reconstitution of *ob/ob* mice with the indicated adenoviruses (n = 10–14). Asterisks in (C) and (D) compare *ob/ob* mice treated with BAD S155D versus GFP adenoviruses.

(E) GTT in C57BL/6J mice subjected to high-fat diet for 10 weeks prior to hepatic reconstitution with the indicated adenoviruses (n = 9). Asterisks in (E) compare HFD mice treated with BAD S155D versus GFP adenoviruses. Error bars show ± SEM. *p < 0.05; **p < 0.01; ***p < 0.001. See also Figure S6.

levels in $Bad^{-/-}$ mice, our results indicate that diminished insulin suppression of HGP in these animals cannot be explained by diminished *Gk* transcription. Considering insulin induction of BAD phosphorylation on S155 and the direct stimulatory effect of the phospho-BAD BH3 domain on GK activity (Szlyk et al., 2014), our data are most consistent with the proposal that defective GK activity in $Bad^{-/-}$ liver, despite stabilized *Gk* mRNA levels, may curtail the full effect of insulin on proper modulation of HGP.

Metabolic Benefits of BAD in Models of Diabetes and Insulin Resistance

The capacity of BAD S155D to counterbalance exaggerated gluconeogenesis in $Bad^{-/-}$ liver warranted examination of its effect in models of diabetes and insulin resistance such as *ob/ob* mice. Hepatic BAD protein levels were comparable in *ob/ob* and control *ob/+* mice despite elevated *Bad* mRNA levels in *ob/ob* animals, indicating that increased transcription of the *Bad* gene does not result in higher protein levels in this context (Figures S6A and S6B). Remarkably, however, BAD phosphorylation on S155 and S136 was significantly diminished in *ob/ob* liver (Figure S6C). These observations further motivated examination of whether expression of a BAD S155D can alter hepatic metabolism in these animals. Hepatic delivery of BAD S155D, but not BAD AAA, significantly ameliorated fasting hyperglycemia in *ob/ob* mice (Figure 7A), which was accompanied by diminished fasting *Pck1* mRNA abundance (Figure 7B). Importantly, glucose levels during PTT were markedly downregulated in *ob/ob* mice reconstituted with BAD S155D adenoviruses so that they were comparable to *ob/+* controls treated with GFP viruses (Figure 7C). BAD S155D expression further resulted in systemic metabolic

Figure 6. Altered Insulin Signaling upon Hepatic Manipulation of BAD and GK

(A) IRS-1-associated PI3K activity in liver of $Bad^{+/+}$ and $Bad^{-/-}$ mice injected with saline or insulin after an overnight fast (n = 10 per genotype).

(B) Phosphorylation of the insulin receptor (IR) and AKT in liver of $Bad^{+/+}$ and $Bad^{-/-}$ mice treated as in (A). Bar graphs quantitate relative insulin induction of IR and AKT phosphorylation (n = 4).

(C and D) Insulin signaling in liver samples isolated from C57BL/6J mice following hepatic knockdown of *Bad* (C) and *Gk* (D). Bar graphs quantitate relative insulin induction of IR, AKT, and GSK-3 phosphorylation (n = 4). Error bars show ± SEM. *p < 0.05; **p < 0.01; ***p < 0.001. See also Figure S5.

benefits marked by improved glucose tolerance in *ob/ob* mice (Figure 7D).

We next set out to determine whether the differential effects of BAD S155D and BAD AAA in *ob/ob* liver parallel their GK-activating capacity. Previous studies have reported an age-dependent progressive decline in hepatic *Gk* mRNA and GK activity in leptin-resistant rodent models (Torres et al., 2009). Importantly, increased GK activity through chemical or genetic approaches improved glucose homeostasis in these models (Grimsby et al., 2003; Torres et al., 2009). Hepatic expression of BAD S155D or BAD AAA variants did not alter *Gk* mRNA levels in *ob/ob* mice (Figure S6D) but had a distinct effect on GK activity. Specifically, BAD S155D increased hepatic GK activity, whereas the BAD AAA variant was ineffective (Figure S6E). Thus, the differential effect of BAD phospho-mutants in hepatic reconstitution of *ob/ob* mice cosegregates with their effect on GK activity.

The *ob/ob* genetic model is a severe model of diabetes with a complex myriad of chronic pathophysiologic perturbations. We also tested the metabolic consequence of BAD in the high-fat diet (HFD) model. Acute hepatic delivery of BAD S155D to wild-type mice after 10 weeks of high-fat feeding effectively improved fasting hyperglycemia and glucose tolerance, while the BAD AAA variant was inert in this setting (Figure 7E). The glucose tolerance test (GTT) profiles of HFD mice treated with BAD S155D were comparable to normal chow (control)-fed mice treated with GFP viruses (Figure 7E).

DISCUSSION

Our combined use of multiple genetic tools, including the *Bad* null and phosphorylation knockin mice, liver-specific *Bad* knockdown, as well as informative BAD mutants enabled biochemical and systemic evaluation of BAD's significance in hepatic substrate metabolism. These studies show that hepatic loss of BAD or interference with its phosphorylation is linked to reduced glycolysis, enhanced FAO, and unrestrained gluconeogenesis. Moreover, BAD deficiency is associated with impaired insulin-mediated suppression of HGP and attenuated insulin signaling. Our collective observations suggest that exaggerated gluconeogenesis in the absence of BAD can be mapped to a combination of altered substrate and energy metabolism, as well as loss of hepatic insulin sensitivity.

BAD's capacity to modulate hepatic glucose utilization and production is regulated by its phosphorylation, which is in turn sensitive to the fed and fasted nutritional states and insulin. When phosphorylated, BAD activates GK, promoting glycolysis and inhibiting FAO. Upon BAD dephosphorylation, glycolysis is diminished, FAO is disinhibited, and pyruvate is preferentially partitioned to gluconeogenesis. These observations are consistent with the possibility that BAD phosphorylation may help mitochondria distinguish the glycolytic versus gluconeogenic source of pyruvate and its metabolic fate. The idea that GK is an important mechanistic component of BAD modulation of hepatic metabolism is supported by two lines of investigation. First, the selective capacity of BAD BH3 variants to modulate hepatic metabolism in both primary hepatocytes and whole-animal liver reconstitution assays cosegregates with their differential GK-activating property. Second, BAD's ability to coordinately regulate hepatic energy metabolism and gluconeogenesis is abolished in the absence of GK, providing evidence in favor of an epistatic relationship between these partner proteins in which GK is a downstream mediator of BAD's metabolic effects.

The notion that the BAD-GK axis is relevant for proper regulation of glycolysis and gluconeogenesis is consistent with several metabolic alterations that are phenocopied when each protein is depleted in the liver, including exaggerated gluconeogenesis and impaired glucose tolerance. Hepatic GK is subject to several regulatory mechanisms, including distinct binding interactions and subcellular localization (Matschinsky, 2009). BAD deficiency does not lead to reduced hepatic GK expression at mRNA or protein levels but is associated with diminished GK activity. Given the multiple mechanisms that converge on hepatic GK regulation, loss of BAD is not expected to recapitulate the full phenotypic spectrum of GK loss of function in the liver. Within this context, the finding that several metabolic alterations are shared between mice with hepatic knockdown of *Bad* and animals with hepatic knockdown of *Gk* is remarkable.

Changes in hepatic metabolism following depletion of BAD or GK also include altered expression of several glycolytic and gluconeogenic genes and a robust transcriptional activation of β-oxidation. This gives rise to the question of how BAD- or GK-dependent changes in hepatic metabolism modify gene expression. Because these changes can be acutely triggered by the knockdown of either BAD or GK, it is likely that select alterations in glucose- or fatty acid-derived metabolites may modulate the activity of glucose- and fatty acid-sensing transcription factors such as carbohydrate-responsive element-binding protein (ChREBP) and nuclear receptors (Agius, 2013; Jump et al., 2013). Another possible scenario is alterations in chromatin- and histone-modifying enzymes that can be modulated by defined metabolites or cellular metabolic state (Kaelin and McKnight, 2013).

Our findings indicate that deregulated gluconeogenesis in the absence of BAD also extends to diminished insulin suppression of HGP. BAD phosphorylation, which can downregulate gluconeogenesis through GK activation (Figures 2C, 2D, S2B, and 4C), is normally induced by insulin. This observation, together with the finding that insulin suppression of HGP is diminished in $Bad^{-/-}$ mice, suggests that BAD may serve as a downstream effector of insulin in modulation of hepatic glucose production. Moreover, hepatic insulin resistance in the absence of BAD is accompanied by changes in insulin signaling. Hepatic nutrient and energy sensing pathways and insulin signaling are tightly integrated (Newgard, 2012; Samuel and Shulman, 2012), and the shared phenotype of reduced insulin signaling upon acute hepatic depletion of BAD or GK predicts a potential interplay between reduced glucose utilization and/or increased FAO and the components of the insulin signaling axis. Notably, precedent for a link between glucose metabolism, ROS, and NADH and the regulation of PI3K-AKT-GSK-3 signaling exists in other tissues (Pelicano et al., 2006; Yeshao et al., 2005). The precise molecular link between BAD- and GK-dependent changes in substrate metabolism and alterations in insulin signaling awaits additional studies.

The observation that hepatic delivery of BAD S155D reinstates proper regulation of gluconeogenesis and allays fasting hyperglycemia in the *ob/ob* and HFD-treated mice provides a powerful

endorsement for the physiologic relevance of BAD phosphoregulation. We have shown that the BAD S155D variant and hydrocarbon-stapled BAD BH3 helices that bear the phosphomimic S155D modification (BAD SAHB compounds) can directly trigger GK activity and stimulate insulin secretion in primary islets (Danial et al., 2008; Szlyk et al., 2014). The studies presented here suggest that in addition to boosting β cell function, BAD BH3 phosphomimic strategies may improve hepatic metabolism. This is consistent with published reports that GK activation imparts benefits to both β cells and hepatocytes. Hepatic GK activation using genetic approaches or pharmacologic tools such as small molecule allosteric GK activators (GKAs) leads to increased glucose utilization, decreased glucose production, amelioration of hyperglycemia, and resistance to HFD (Ferre et al., 1996; Grimsby et al., 2003; Torres et al., 2009). However, these benefits have to be carefully leveraged against potential risk of hypoglycemia and hyperlipidemia associated with chronic GK activation above physiologic levels (Meininger et al., 2011). With advances in the development of different classes of GKAs that may elicit distinct mechanisms of action and the possibility of combination therapy with other antidiabetic agents, the benefits of GK activation may ultimately outweigh these drawbacks (Matschinsky, 2009). Within this context, it is important to note that the mechanism by which the phospho-BAD BH3 helix activates GK is distinct from allosteric GKAs (Szlyk et al., 2014), suggesting that phospho-BAD BH3 mimetic compounds may define a separate class of GKAs. The findings reported here highlight the potential therapeutic utility of phospho-BAD BH3 mimetic strategies in diabetes and metabolic syndrome.

EXPERIMENTAL PROCEDURES

Mice

Bad$^{-/-}$ and S155A knockin mice have been previously described (Danial et al., 2008). These mice have been bred into the C57BL/6J genetic background for at least 14 generations and validated by genome scanning to be 99.9% congenic with C57BL/6J. Conditional *Gk* mice (*Gk*$^{lox/lox}$) were a generous gift of Dr. Mark Magnuson (Vanderbilt University) (Postic et al., 1999). C57BL/6J *alb-cre* mice and *ob/ob* mice were purchased from Jackson Laboratory and Taconic, respectively. Mice received a standard chow or high-fat diet (55% fat energy, TD93075, Harlan Laboratories) and were housed in a barrier facility with 12 hr light and dark cycles. Unless otherwise indicated, male mice at 10–12 weeks of age were used. All animal procedures were approved by the Institutional Animal Care and Use Committee of Dana-Farber Cancer Institute and Yale University School of Medicine.

Metabolic Studies

PTT, GTT, basal metabolic characterization, and euglycemic-hyperinsulinemic clamps were performed as previously described (Choi et al., 2007; Danial et al., 2008; Lin et al., 2004). Adenoviral transduction was carried out as described in the Supplemental Experimental Procedures.

Mitochondrial Respirometry

OCR was measured in intact hepatocytes in real time using the XF24 Extracellular Flux Analyzer and the XF24 v1.5.0.69 software (Seahorse Bioscience). Cells were seeded on collagen-coated XF24 V7 plates at 4 × 10^4 cells/well, allowed to attach for at least 2 hr, rinsed once, and kept in 600 μl of sodium bicarbonate-free M199 medium supplemented with 1% BSA, 1 μM dexamethasone, and 12 μM forskolin. After baseline measurements, additions were delivered in the following order through the instrument's individual injection ports: substrates (lactate and pyruvate or palmitate), ADP, and oligomycin. L-lactate (Sigma) and sodium pyruvate (Cellgro, Mediatech) were injected at 10 and 1 mM, respectively. Sodium palmitate (Sigma) was injected at 200 μM together with 10 mM L-malate (Sigma). When palmitate was tested, 0.5 mM carnitine (Sigma) was included in the incubation and equilibration medium. Where indicated, etomoxir (Sigma) was included in incubation and equilibration medium at 50 μM final concentration. After addition of the substrates, 5 mM ADP (Sigma) was injected to drive maximum respiration. Lastly, 1 μM oligomycin (Calbiochem) was injected to derive the portion of OCR used for ATP synthesis. OCR values in Figures 3 and 4 represent the difference between the maximal rate in the presence of ADP and the rate after addition of oligomycin, thus indicating ATP production by mitochondrial oxidative phosphorylation. Additional experimental details and a summary table of OCR values in the presence and absence of ADP for all substrates and genotypes tested are provided in Table S1 and the Supplemental Experimental Procedures.

Statistical Analysis

Data are presented as mean ± SEM of the indicated number of independent experiments or mice per genotype. Statistical significance among the groups was tested with unpaired or paired Student's t test and ANOVA when appropriate. Differences were considered significant at $p < 0.05$.

SUPPLEMENTAL INFORMATION

Supplemental Information includes Supplemental Experimental Procedures, six figures, and one table and can be found with this article online at http://dx.doi.org/10.1016/j.cmet.2013.12.001.

ACKNOWLEDGMENTS

We thank J. Quijada for technical assistance and animal husbandry; J. Lemasters for advice on OCR studies; and B. Lowell, P. Puigserver, members of the Spiegelman laboratory, L. Agius, and F. Matschinsky for helpful discussions. A.G.-C. and L.G.-H. were supported by postdoctoral fellowships from the Ministerio de Educación y Ciencia (MEC, Spain). M.A.O. was supported by a postdoctoral fellowship from the Juvenile Diabetes Research Foundation. N.N.D. is a recipient of the Burroughs Wellcome Fund Career Award in Biomedical Sciences. This work was supported by the US National Institutes of Health grants K01CA10659 (N.N.D.), R01DK078081 (N.N.D.), R01 DK-40936 (G.I.S.), U24 DK-059635 (G.I.S.), and R01DK083567 (Y.-B.K.) and the Korea Healthcare technology R&D Project A102060, Ministry for Health, Welfare & Family Affairs, Republic of Korea (C.S.C.).

Received: September 18, 2012
Revised: October 7, 2013
Accepted: December 5, 2013
Published: February 4, 2014

REFERENCES

Agius, L. (2008). Glucokinase and molecular aspects of liver glycogen metabolism. Biochem. J. *414*, 1–18.

Agius, L. (2013). High-carbohydrate diets induce hepatic insulin resistance to protect the liver from substrate overload. Biochem. Pharmacol. *85*, 306–312.

Barzilai, N., Hawkins, M., Angelov, I., Hu, M., and Rossetti, L. (1996). Glucosamine-induced inhibition of liver glucokinase impairs the ability of hyperglycemia to suppress endogenous glucose production. Diabetes *45*, 1329–1335.

Bechmann, L.P., Gastaldelli, A., Vetter, D., Patman, G.L., Pascoe, L., Hannivoort, R.A., Lee, U.E., Fiel, I., Muñoz, U., Ciociaro, D., et al. (2012). Glucokinase links Krüppel-like factor 6 to the regulation of hepatic insulin sensitivity in nonalcoholic fatty liver disease. Hepatology *55*, 1083–1093.

Burgess, S.C., He, T., Yan, Z., Lindner, J., Sherry, A.D., Malloy, C.R., Browning, J.D., and Magnuson, M.A. (2007). Cytosolic phosphoenolpyruvate carboxykinase does not solely control the rate of hepatic gluconeogenesis in the intact mouse liver. Cell Metab. *5*, 313–320.

Choi, C.S., Savage, D.B., Abu-Elheiga, L., Liu, Z.X., Kim, S., Kulkarni, A., Distefano, A., Hwang, Y.J., Reznick, R.M., Codella, R., et al. (2007). Continuous fat oxidation in acetyl-CoA carboxylase 2 knockout mice

increases total energy expenditure, reduces fat mass, and improves insulin sensitivity. Proc. Natl. Acad. Sci. USA *104*, 16480–16485.

Clément, K., Pueyo, M.E., Vaxillaire, M., Rakotoambinina, B., Thuillier, F., Passa, P., Froguel, P., Robert, J.J., and Velho, G. (1996). Assessment of insulin sensitivity in glucokinase-deficient subjects. Diabetologia *39*, 82–90.

Copps, K.D., and White, M.F. (2012). Regulation of insulin sensitivity by serine/threonine phosphorylation of insulin receptor substrate proteins IRS1 and IRS2. Diabetologia *55*, 2565–2582.

Cournarie, F., Azzout-Marniche, D., Foretz, M., Guichard, C., Ferre, P., and Foufelle, F. (1999). The inhibitory effect of glucose on phosphoenolpyruvate carboxykinase gene expression in cultured hepatocytes is transcriptional and requires glucose metabolism. FEBS Lett. *460*, 527–532.

Danial, N.N. (2008). BAD: undertaker by night, candyman by day. Oncogene *27* (*Suppl 1*), S53–S70.

Danial, N.N., Gramm, C.F., Scorrano, L., Zhang, C.Y., Krauss, S., Ranger, A.M., Datta, S.R., Greenberg, M.E., Licklider, L.J., Lowell, B.B., et al. (2003). BAD and glucokinase reside in a mitochondrial complex that integrates glycolysis and apoptosis. Nature *424*, 952–956.

Danial, N.N., Walensky, L.D., Zhang, C.Y., Choi, C.S., Fisher, J.K., Molina, A.J., Datta, S.R., Pitter, K.L., Bird, G.H., Wikstrom, J.D., et al. (2008). Dual role of proapoptotic BAD in insulin secretion and beta cell survival. Nat. Med. *14*, 144–153.

Ferre, T., Pujol, A., Riu, E., Bosch, F., and Valera, A. (1996). Correction of diabetic alterations by glucokinase. Proc. Natl. Acad. Sci. USA *93*, 7225–7230.

Grimsby, J., Sarabu, R., Corbett, W.L., Haynes, N.E., Bizzarro, F.T., Coffey, J.W., Guertin, K.R., Hilliard, D.W., Kester, R.F., Mahaney, P.E., et al. (2003). Allosteric activators of glucokinase: potential role in diabetes therapy. Science *301*, 370–373.

Gustafson, L.A., Neeft, M., Reijngoud, D.J., Kuipers, F., Sauerwein, H.P., Romijn, J.A., Herling, A.W., Burger, H.J., and Meijer, A.J. (2001). Fatty acid and amino acid modulation of glucose cycling in isolated rat hepatocytes. Biochem. J. *358*, 665–671.

Hakimi, P., Johnson, M.T., Yang, J., Lepage, D.F., Conlon, R.A., Kalhan, S.C., Reshef, L., Tilghman, S.M., and Hanson, R.W. (2005). Phosphoenolpyruvate carboxykinase and the critical role of cataplerosis in the control of hepatic metabolism. Nutr. Metab. (Lond) *2*, 33.

Jump, D.B., Tripathy, S., and Depner, C.M. (2013). Fatty acid-regulated transcription factors in the liver. Annu. Rev. Nutr. *33*, 249–269.

Kaelin, W.G., Jr., and McKnight, S.L. (2013). Influence of metabolism on epigenetics and disease. Cell *153*, 56–69.

Kim, T.H., Kim, H., Park, J.M., Im, S.S., Bae, J.S., Kim, M.Y., Yoon, H.G., Cha, J.Y., Kim, K.S., and Ahn, Y.H. (2009). Interrelationship between liver X receptor alpha, sterol regulatory element-binding protein-1c, peroxisome proliferator-activated receptor gamma, and small heterodimer partner in the transcriptional regulation of glucokinase gene expression in liver. J. Biol. Chem. *284*, 15071–15083.

Lin, H.V., and Accili, D. (2011). Hormonal regulation of hepatic glucose production in health and disease. Cell Metab. *14*, 9–19.

Lin, J., Wu, P.H., Tarr, P.T., Lindenberg, K.S., St-Pierre, J., Zhang, C.Y., Mootha, V.K., Jäger, S., Vianna, C.R., Reznick, R.M., et al. (2004). Defects in adaptive energy metabolism with CNS-linked hyperactivity in PGC-1alpha null mice. Cell *119*, 121–135.

Magnuson, M.A., She, P., and Shiota, M. (2003). Gene-altered mice and metabolic flux control. J. Biol. Chem. *278*, 32485–32488.

Matschinsky, F.M. (2009). Assessing the potential of glucokinase activators in diabetes therapy. Nat. Rev. Drug Discov. *8*, 399–416.

Meininger, G.E., Scott, R., Alba, M., Shentu, Y., Luo, E., Amin, H., Davies, M.J., Kaufman, K.D., and Goldstein, B.J. (2011). Effects of MK-0941, a novel glucokinase activator, on glycemic control in insulin-treated patients with type 2 diabetes. Diabetes Care *34*, 2560–2566.

Newgard, C.B. (2012). Interplay between lipids and branched-chain amino acids in development of insulin resistance. Cell Metab. *15*, 606–614.

Oosterveer, M.H., Mataki, C., Yamamoto, H., Harach, T., Moullan, N., van Dijk, T.H., Ayuso, E., Bosch, F., Postic, C., Groen, A.K., et al. (2012). LRH-1-dependent glucose sensing determines intermediary metabolism in liver. J. Clin. Invest. *122*, 2817–2826.

Payne, V.A., Arden, C., Wu, C., Lange, A.J., and Agius, L. (2005). Dual role of phosphofructokinase-2/fructose bisphosphatase-2 in regulating the compartmentation and expression of glucokinase in hepatocytes. Diabetes *54*, 1949–1957.

Pelicano, H., Xu, R.H., Du, M., Feng, L., Sasaki, R., Carew, J.S., Hu, Y., Ramdas, L., Hu, L., Keating, M.J., et al. (2006). Mitochondrial respiration defects in cancer cells cause activation of Akt survival pathway through a redox-mediated mechanism. J. Cell Biol. *175*, 913–923.

Postic, C., Shiota, M., Niswender, K.D., Jetton, T.L., Chen, Y., Moates, J.M., Shelton, K.D., Lindner, J., Cherrington, A.D., and Magnuson, M.A. (1999). Dual roles for glucokinase in glucose homeostasis as determined by liver and pancreatic beta cell-specific gene knock-outs using Cre recombinase. J. Biol. Chem. *274*, 305–315.

Pryor, H.J., Smyth, J.E., Quinlan, P.T., and Halestrap, A.P. (1987). Evidence that the flux control coefficient of the respiratory chain is high during gluconeogenesis from lactate in hepatocytes from starved rats. Implications for the hormonal control of gluconeogenesis and action of hypoglycaemic agents. Biochem. J. *247*, 449–457.

Rizza, R.A. (2010). Pathogenesis of fasting and postprandial hyperglycemia in type 2 diabetes: implications for therapy. Diabetes *59*, 2697–2707.

Rossetti, L., Chen, W., Hu, M., Hawkins, M., Barzilai, N., and Efrat, S. (1997). Abnormal regulation of HGP by hyperglycemia in mice with a disrupted glucokinase allele. Am. J. Physiol. *273*, E743–E750.

Rothman, D.L., Magnusson, I., Katz, L.D., Shulman, R.G., and Shulman, G.I. (1991). Quantitation of hepatic glycogenolysis and gluconeogenesis in fasting humans with 13C NMR. Science *254*, 573–576.

Saltiel, A.R., and Kahn, C.R. (2001). Insulin signalling and the regulation of glucose and lipid metabolism. Nature *414*, 799–806.

Samuel, V.T., and Shulman, G.I. (2012). Mechanisms for insulin resistance: common threads and missing links. Cell *148*, 852–871.

Satapati, S., Sunny, N.E., Kucejova, B., Fu, X., He, T.T., Méndez-Lucas, A., Shelton, J.M., Perales, J.C., Browning, J.D., and Burgess, S.C. (2012). Elevated TCA cycle function in the pathology of diet-induced hepatic insulin resistance and fatty liver. J. Lipid Res. *53*, 1080–1092.

Scott, D.K., O'Doherty, R.M., Stafford, J.M., Newgard, C.B., and Granner, D.K. (1998). The repression of hormone-activated PEPCK gene expression by glucose is insulin-independent but requires glucose metabolism. J. Biol. Chem. *273*, 24145–24151.

Szlyk, B., Braun, C.R., Ljubicic, S., Patton, E., Bird, G.H., Osundiji, M.A., Matschinsky, F.M., Walensky, L.D., and Danial, N.N. (2014). A phospho-BAD BH3 helix activates glucokinase by a mechanism distinct from that of allosteric activators. Nat. Struct. Mol. Biol. *21*, 36–42.

Torres, T.P., Catlin, R.L., Chan, R., Fujimoto, Y., Sasaki, N., Printz, R.L., Newgard, C.B., and Shiota, M. (2009). Restoration of hepatic glucokinase expression corrects hepatic glucose flux and normalizes plasma glucose in zucker diabetic fatty rats. Diabetes *58*, 78–86.

Velho, G., Petersen, K.F., Perseghin, G., Hwang, J.H., Rothman, D.L., Pueyo, M.E., Cline, G.W., Froguel, P., and Shulman, G.I. (1996). Impaired hepatic glycogen synthesis in glucokinase-deficient (MODY-2) subjects. J. Clin. Invest. *98*, 1755–1761.

Wu, C., Okar, D.A., Stoeckman, A.K., Peng, L.J., Herrera, A.H., Herrera, J.E., Towle, H.C., and Lange, A.J. (2004). A potential role for fructose-2,6-bisphosphate in the stimulation of hepatic glucokinase gene expression. Endocrinology *145*, 650–658.

Yamada, K., and Noguchi, T. (1999). Nutrient and hormonal regulation of pyruvate kinase gene expression. Biochem. J. *337*, 1–11.

Yeshao, W., Gu, J., Peng, X., Nairn, A.C., and Nadler, J.L. (2005). Elevated glucose activates protein synthesis in cultured cardiac myocytes. Metabolism *54*, 1453–1460.

Cell Metabolism, Volume *19*

Supplemental Information

Regulation of Hepatic Energy Metabolism and Gluconeogenesis by BAD

Alfredo Giménez-Cassina, Luisa Garcia-Haro, Cheol Soo Choi, Mayowa A. Osundiji, Elizabeth A. Lane, Hu Huang, Muhammed A. Yildirim, Benjamin Szlyk, Jill K. Fisher, Klaudia Polak, Elaura Patton, Jessica Wiwczar, Marina Godes, Dae Ho Lee, Kirsten Robertson, Sheene Kim, Ameya Kulkarni, Alberto Distefano, Varman Samuel, Gary Cline, Young-Bum Kim, Gerald I. Shulman, and Nika N. Danial

SUPPLEMENTAL DATA

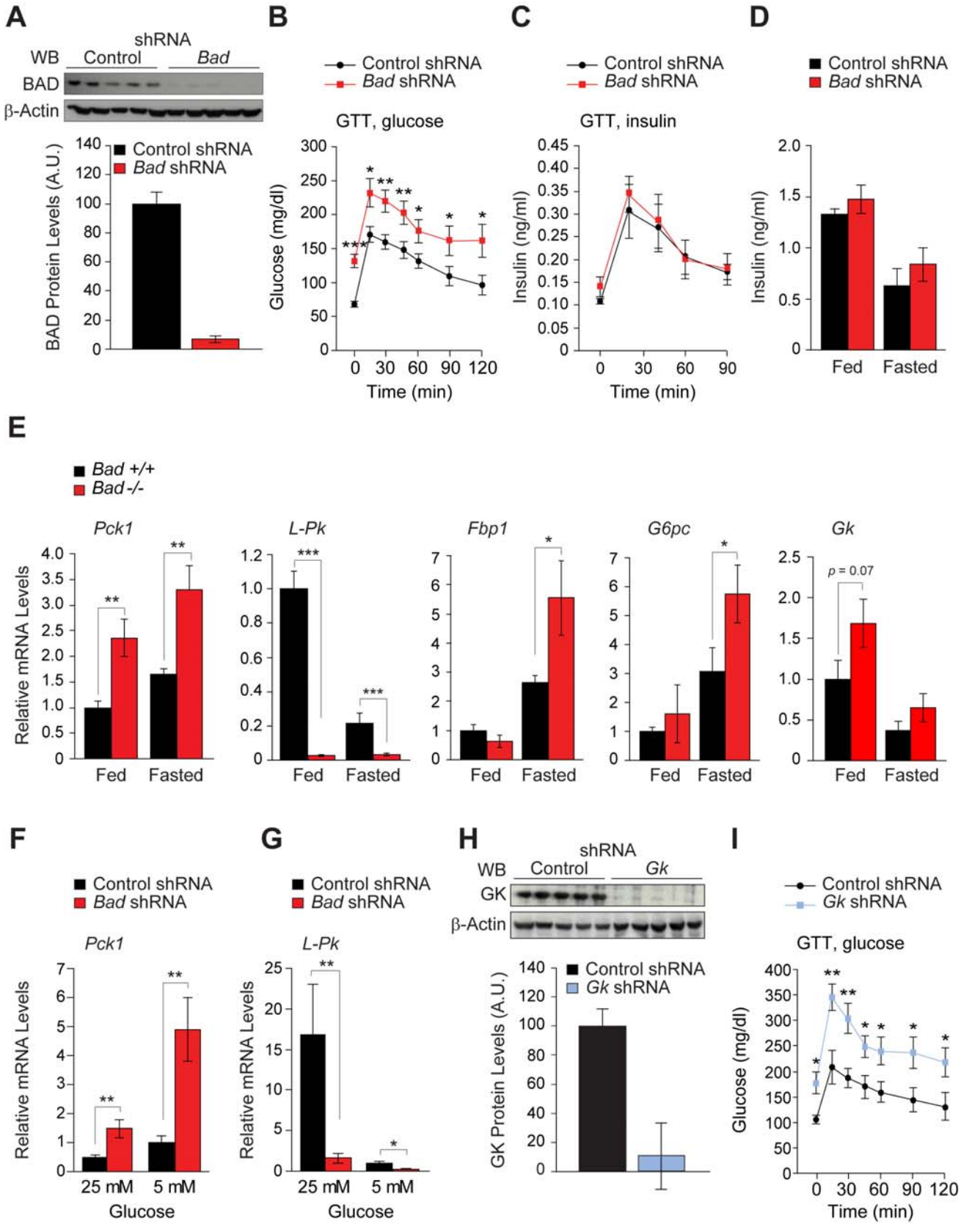

Giménez-Cassina, et al. Figure S1

Figure S1, related to Figure 1. Modulation of hepatic glucose metabolism by BAD. (A) Hepatic BAD protein levels in C57BL/6J mice 5 days after tail vein delivery of control or *Bad* shRNA adenoviruses. (B-C) Blood glucose (B) and insulin levels (C) during i.p. GTT in C57BL/6J mice treated as in (A) (n=5-8). (D) Serum insulin levels in fed and overnight-fasted C57BL/6J mice after hepatic knockdown of *Bad* (n=10). (E) Relative hepatic mRNA levels of glycolytic (*L-Pk*, *Gk*) and gluconeogenic (*Pck1*, *Fbp1*, *G6pc*) genes in fed and overnight-fasted *Bad* +/+ and -/- mice (n=5). (F-G) Relative levels of *Pck1* (F) and *L-Pk* (G) mRNAs in primary hepatocytes incubated with high or low glucose concentrations for 24 hr after *Bad* knockdown (n=4-5 independent hepatocyte cultures). (H) Hepatic GK protein levels in C57BL/6J mice 5 days after tail vein delivery of control or *Gk* shRNA adenoviruses. (I) Blood glucose during i.p. GTT in C57BL/6J mice treated as in (H) (n=5). Error bars, ± SEM. *$p < 0.05$; **$p < 0.01$; ***$p < 0.001$.

A

BAD BH3 Variants	GK-Activating Capacity	Binding to BCL-2 Family Partners
Wild-type L W A A Q R Y G R E L R R M S D E F E G S F K G L	+	+
S155D L W A A Q R Y G R E L R R M D D E F E G S F K G L	+	-
S155A L W A A Q R Y G R E L R R M A D E F E G S F K G L	-	+
AAA (L151A, S155A, D156A) L W A A Q R Y G R E A R R M A A E F E G S F K G L	-	-

B

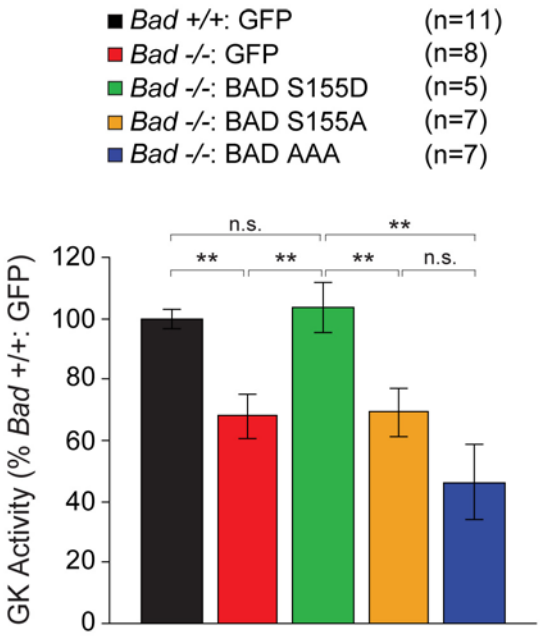

Figure S2, related to Figure 2. BAD's hepatic function is modulated by its phosphorylation status. (A) BAD phospho-variants used in reconstitution studies. The effect of each mutation on BAD's dual functions or interaction partners is summarized. (B) Hepatic GK activity in *Bad* +/+ and -/- mice after tail vein delivery of the indicated adenoviruses. Error bars, ± SEM. **p < 0.01; n.s., non-significant.

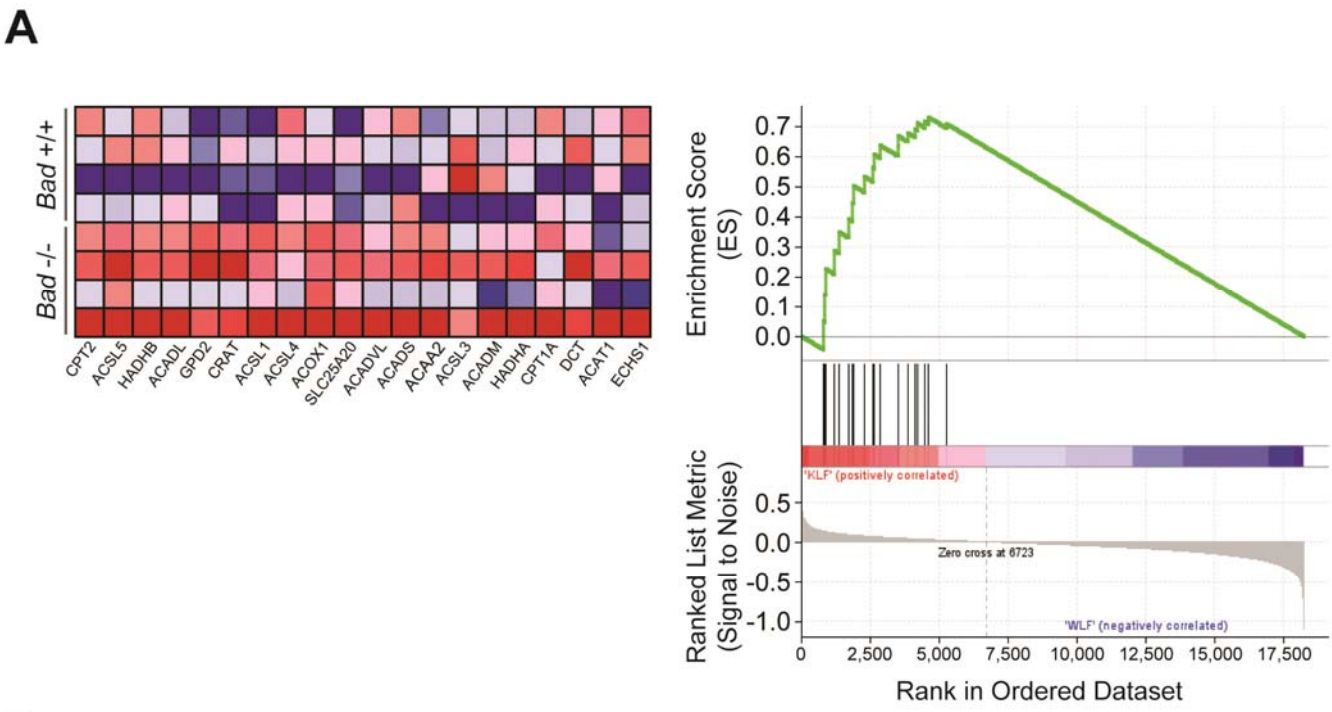

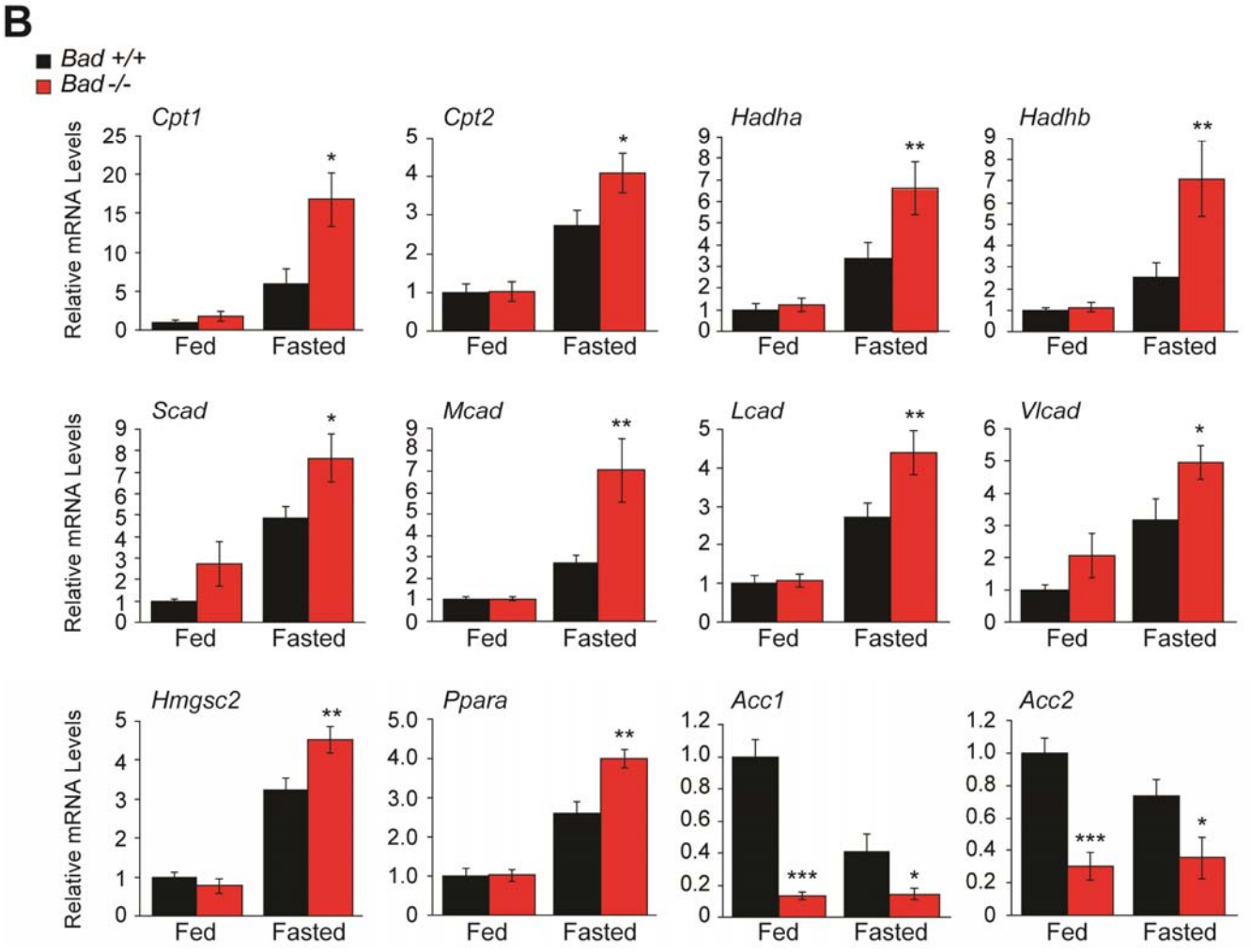

Giménez-Cassina, et al. Figure S3

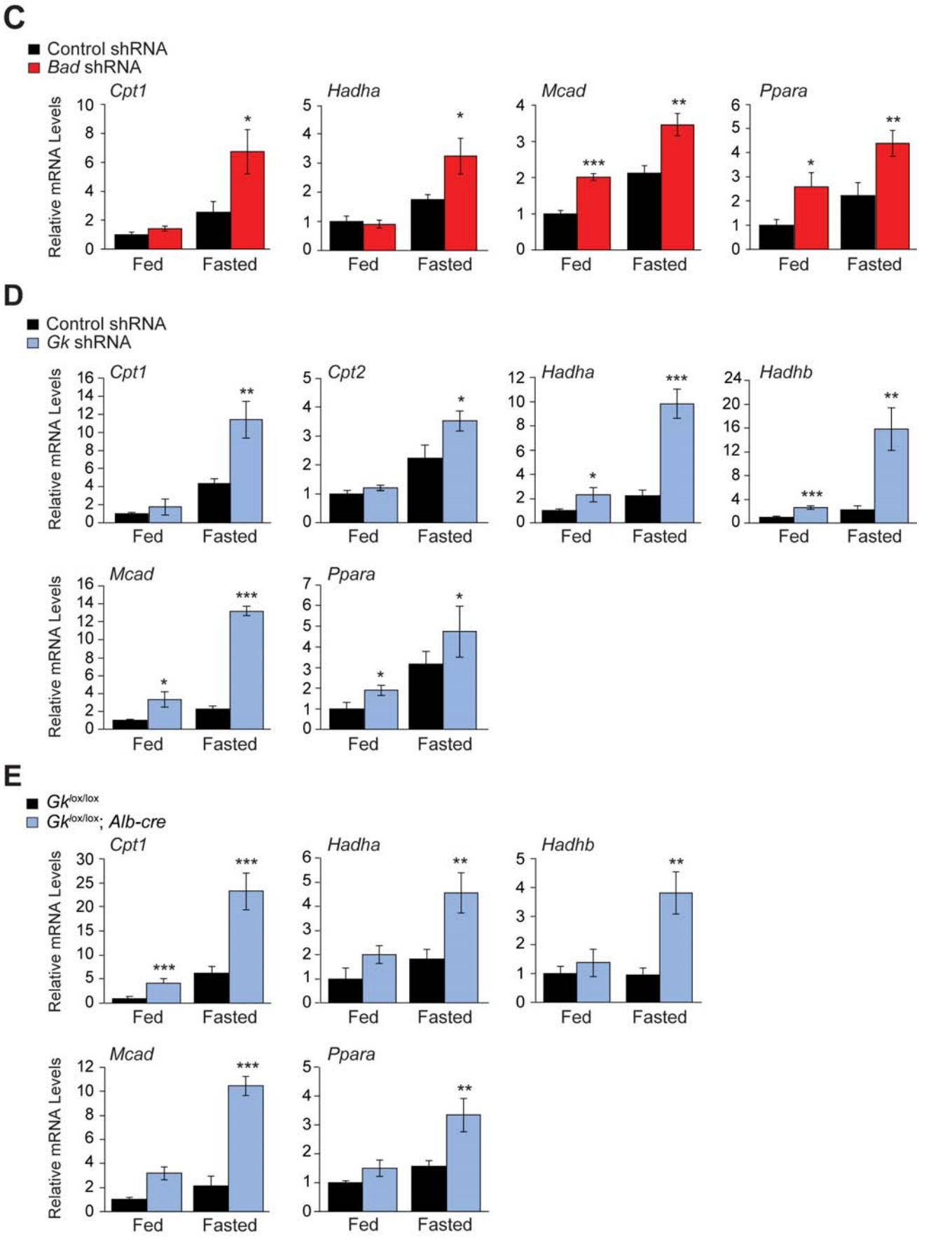

Giménez-Cassina, et al. Figure S3

Figure S3, related to Figure 3. Changes in the expression of genes involved in fatty acid metabolism following hepatic manipulation of BAD and GK. (A) Gene set enrichment analysis of mitochondrial β-oxidation in 24 hr-fasted *Bad* +/+ and -/- liver (n=4-5). (B-C) mRNA abundance of fatty acid metabolism genes in liver samples derived from fed and fasted *Bad* +/+ and -/- mice (B) and mice subjected to hepatic knockdown of *Bad* (C) (n=4-5). (D-E) mRNA abundance of β-oxidation genes in liver samples derived from mice treated with *Gk* shRNA adenoviruses (D) and liver-specific *Gk* null mice (E) (n=5). Error bars, ± SEM. *p < 0.05; **p < 0.01; ***p < 0.001.

Abbreviations: *Cpt*, carnitine palmitoyl transferase; *Scad*, *Mcad*, *Lcad* and *Vlcad*, short-, medium-, long-, very long-acyl-CoA dehydrogenase; *Hadh*, hydroxyacyl-CoA dehydrogenase (component of the mitochondrial trifunctional protein); *Acc*, acetyl-CoA carboxylase; *Hmgcs2*, mitochondrial 3-hydroxy-3-methylglutaryl-CoA synthase 2; *Ppara*, peroxisome proliferator-activated receptor alpha.

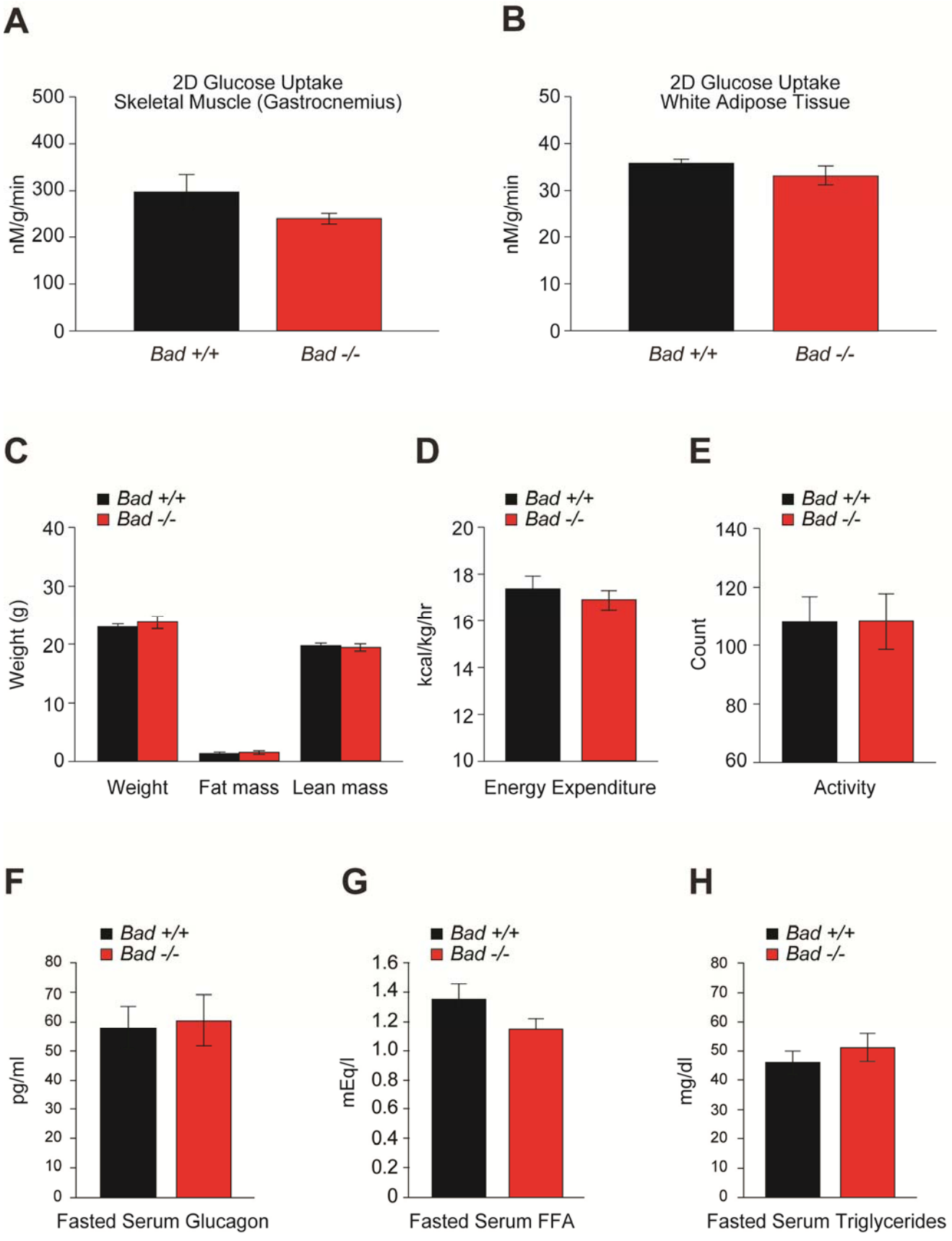

Giménez-Cassina, et al. Figure S4

Figure S4, related to Figure 5. Peripheral insulin action and additional metabolic parameters in *Bad* +/+ and -/- mice. (A-B) Peripheral insulin action as measured by glucose uptake in skeletal muscle (A) and white adipose tissues (B) in *Bad* +/+ and -/- mice subjected to euglycemic-hyperinsulinemic clamp analysis as in Figure 5 (n=7-9). (C-E) Body weight, lean and fat mass (C), energy expenditure (D), and activity (E) in *Bad* +/+ and -/- mice (n=7-9). (F-H) Fasting levels of serum glucagon (F), FFA (G), and Triglycerides (H) in *Bad* +/+ and -/- mice (n=5-9). Error bars, ± SEM.

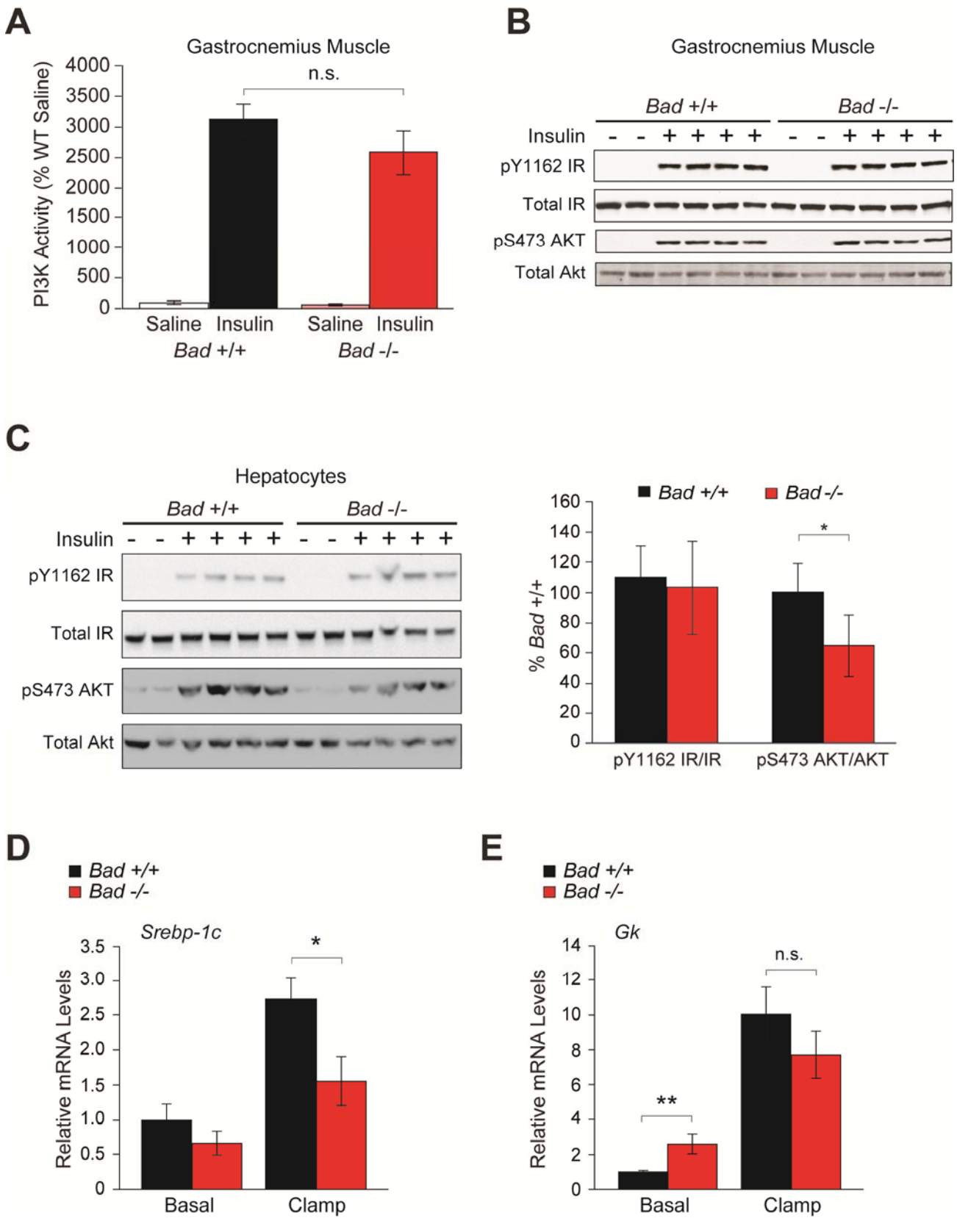

Giménez-Cassina, et al. Figure S5

Figure S5, related to Figure 6. Insulin signaling in the absence of BAD. (A) IRS-1-associated PI3K activity in muscle of *Bad* +/+ and -/- mice injected with saline or 0.1 U/g insulin after an overnight fast (n=10 mice per genotype). (B) Phosphorylation of the insulin receptor (IR) and AKT in skeletal muscle of *Bad* +/+ and -/- mice treated as in (A) (n=4). (C) Insulin signaling in primary *Bad* +/+ and -/- hepatocyte cultures. Bar graphs quantitate relative insulin induction of IR and AKT phosphorylation (n=4). (D-E) Relative hepatic mRNA abundance of *Srebp1c* (D) and *Gk* (E) in *Bad* -/- and *Bad* +/+ mice subjected to euglycemic-hyperinsulinemic clamp as in Figure 5 (n=6 mice per condition). Error bars, mean ± SEM. *$p < 0.05$; **$p < 0.01$; n.s., non-significant.

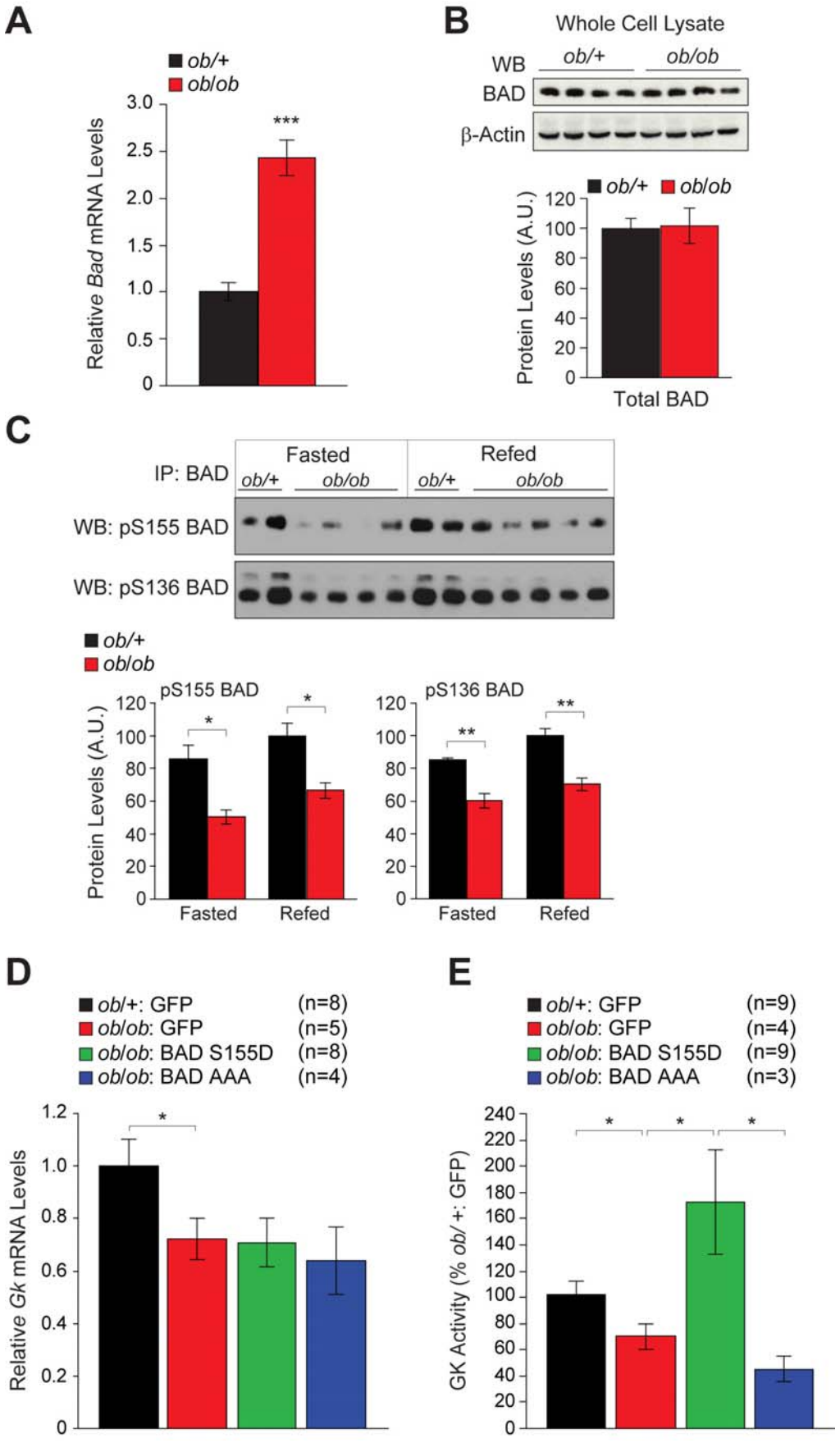

Giménez-Cassina, et al. Figure S6

Figure S6, related to Figure 7. Metabolic effects of BAD in *ob*/*ob* liver. (A) Hepatic mRNA abundance of *Bad* in *ob*/+ and *ob*/*ob* mice (n=6). (B) Immunoblot analysis of total BAD levels in whole cell lysates prepared from *ob*/*ob* and *ob*/+ liver samples. (C) Immunoblot analysis and quantification of relative BAD phosphorylation in liver samples derived from *ob*/*ob* and *ob*/+ mice fasted for 24 hr and refed for 1 hr. BAD was immunoprecipitated with anti-BAD antibody and western blotted with phospho-specific antibodies to pS155 and pS136 BAD. (D) Hepatic *Gk* mRNA levels in ~25-week-old *ob*/+ and *ob*/*ob* mice after tail vein delivery of the indicated adenoviruses (n=4-8 independent mice per condition). (E) Hepatic GK activity in *ob*/*ob* mice after tail vein delivery of the indicated adenoviruses (n=3-9 mice per condition). Error bars, ± SEM. *$p < 0.05$; **$p < 0.01$; ***$p < 0.001$.

		Mean ± SEM		p value		
Figure	**Genotype**	**Without ADP**	**With ADP**		**Without ADP**	**With ADP**
3A (Lac/Pyr)	*Bad* +/+: GFP	408.69 ± 57.89	655.23 ± 84.88	*Bad* +/+: GFP vs. *Bad* -/-: GFP	*	**
	Bad -/-: GFP	620.44 ± 73.4	1021.85 ± 125.08	*Bad* -/-: GFP vs. S155D	**	**
	Bad -/-: BAD S155D	380.44 ± 45.28	582.28 ± 65.49	*Bad* -/-: GFP vs. BAD AAA	n.s.	n.s.
	Bad -/-: BAD AAA	761.07 ± 90.66	1250.34 ± 148.32	*Bad* -/-: BAD S155D vs. BAD AAA	***	***
3B (Palmitate)	*Bad* +/+	259.25 ± 25.46	501.34 ± 45.54	*Bad* +/+ vs. *Bad* -/-	***	***
	Bad -/-	597.32 ± 58.60	1022.36 ± 105.05			
3C (Lac/Pyr)	*Bad* +/+	431.21 ± 74.93	488.97± 57.24	*Bad* +/+ vs. *Bad* -/-	*	***
	Bad -/-	679.27 ± 55.92	1161.25 ± 54.51	*Bad* +/+: minus vs. plus Etx	*	**
	Bad +/+ plus Etx	226.06 ± 39.39	289.34 ± 46.63	*Bad* -/-: minus vs. plus Etx	***	***
	Bad -/- plus Etx	416.56 ± 46.71	578.46 ± 45.26	*Bad* +/+ plus Etx vs. *Bad* -/- plus Etx	**	***
4A (Lac/Pyr)	$GK^{lox/lox}$	285.01 ± 21.29	358.92 ± 28.49	$GK^{lox/lox}$ vs. $GK^{lox/lox}$; *Alb-cre*	**	**
	$GK^{lox/lox}$; *Alb-cre*	1385.08 ± 384.75	1479.88 ± 383.79			
4A (Palmitate)	$GK^{lox/lox}$	231.22 ± 19.79	326.97 ± 20.58	$GK^{lox/lox}$ vs. $GK^{lox/lox}$; *Alb-cre*	**	**
	$GK^{lox/lox}$; *Alb-cre*	815.01 ± 201.08	1127.75 ± 247.84			
4B (Lac/Pyr)	$GK^{lox/lox}$: GFP	616.83 ± 71.09	805.96 ± 145.87	$GK^{lox/lox}$ vs. $GK^{lox/lox}$; *Alb-cre*: GFP	***	***
	$GK^{lox/lox}$; *Alb-cre*: GFP	1510.14 ± 197.23	2470.43 ± 276.37			
	$GK^{lox/lox}$; *Alb-cre*: BAD S155D	1737.45 ± 234.959	2539.64 ± 277.88			

Table S1, related to Figures 3 and 4. Summary of oligomycin-inhibitable portion of OCR in the absence and presence of ADP. OCR values in the absence and presence of ADP are shown for all substrates and genotypes tested in Figures 3 and 4. As expected, the OCR values were lower in the absence of ADP than in its presence, however, statistical significance held across comparisons regardless of the absence or presence of ADP. Main Figures 3 and 4 show OCR values in the presence of ADP. *$p < 0.05$; **$p < 0.01$; ***$p < 0.001$; n.s., non-significant.

SUPPLEMENTAL EXPERIMENTAL PROCEDURES

Adenovirus production and viral transduction. The BAD S155D, S155A, and AAA mutations were made using standard site directed mutagenesis techniques to substitute aspartic acid or alanine for S155 (amino acid enumeration based on mouse BAD protein sequence) or to generate a triple-alanine substitution for L151, S155 and D156 within the BAD BH3 domain (BAD AAA). Recombinant GFP, BAD WT, BAD S155D, S155A, and BAD AAA adenoviruses were generated using the pAdEasy system (Stratagene). Adenoviruses carrying *Bad* shRNA or scrambled control were constructed using the Adeno-X Expression Systems 2 with Creator Technology (Clontech). Briefly, 19 bp sequences based on the BAD coding sequence were designed using Block-it RNAi designer software (Invitrogen). Oligonucleotides were then designed according to the knockout clone and confirm PCR kit (Clontech), and cloned into RNAi-Ready pSIREN-DNR-Ds Red-Express Donor vector. Adenoviruses carrying *Gk* shRNA were a kind gift of Dr. Christopher Newgard (Duke University) (Bain et al., 2004). All virus amplification, purification, titration and verification were done using the services of ViraQuest Inc. (North Liberty, IA). Adenoviral transduction of hepatocyte cultures was carried out 24-48 hr after plating at a viral dose of $4x10^6$ pfu/ml for 3 hr. For hepatic reconstitution or knockdown assays, mice were injected with a viral dose of $3x10^8$ pfu/g of body weight via tail vein.

Primary hepatocyte cultures and treatments. Primary hepatocyte isolation and cultures were carried out as previously described (Matsumoto et al., 2007). Cells were starved in serum-free M199 (Invitrogen) for 40 hr prior to dexamethasone/forskolin treatment. For assessment of lactate production, hepatocytes were plated at $5.5x10^5$ cells/ml and incubated in serum-free M199 supplemented with 0.2% BSA for 4 hr and then switched to serum-free M199 containing 0.2% BSA without or with 25 mM glucose for up to 24 hr. 100 µl aliquots of the medium were collected at the indicated times for lactate measurement as previously described (Ferre et al., 1996) and normalized to the protein content of hepatocytes. For glucose production assays, hepatocytes were cultured in M199 medium containing 0.5% BSA. Glucose production in the presence of lactate and pyruvate was assessed as previously described (Yoon et al., 2001). Values were normalized to protein content.

Hepatic GK activity assays. Whole livers were extracted from mice administered with the indicated adenoviruses and flash frozen in liquid nitrogen. Samples were homogenized in buffer containing 220 mM mannitol, 70 mM sucrose, 20 mM HEPES pH 7.4, 0.5 mM EGTA, and 0.1%

defatted BSA that was supplemented with complete protease inhibitor cocktail (Roche). Samples were centrifuged at 600 x g for 10 min at 4°C to pellet large matter and separate a layer of fat from the homogenate, which was aspirated prior to measuring the protein concentration. Samples were diluted to 1 mg/mL total protein concentration, and assayed in a G6PDH-coupled reaction measuring the formation of NADH at 340 nm in a Costar 3596 plate at 37°C using a SpectraMax M5 microplate reader (Molecular Devices). Each well contained 400 µg of protein, 100 mM HEPES pH 7.4, 150 mM KCl, 6 mM $MgCl_2$, 5 mM ATP, 1 mM NAD, 1 mM DTT, 0.5% BSA, 2.5 units G6PDH, and either high (100 mM) or low (0.5 mM) glucose. Absorbance was recorded every two min and the change in absorbance per min was calculated using data between 10 and 30 min, where the change in absorbance was linear. Experiments were performed in triplicate. To determine the contribution from glucokinase alone, baseline-subtracted rates were calculated by subtracting the mean rate of reaction in low glucose from the mean rate of reaction in high glucose for each sample. To normalize the data, the baseline-subtracted rate of each sample was then divided by average of the baseline-subtracted rates of control mice injected with GFP [*Bad* +/+: GFP (Figure S2B) or *ob*/+: GFP (Figure S6E) from the same experiment.

Mitochondrial respirometry in intact hepatocytes. OCR was measured in intact hepatocytes in real time using the XF24 extracellular flux analyzer and the XF24 v1.5.0.69 software (Seahorse Biosciences) (Wu et al., 2007). Hepatocytes were counted using a trypan blue exclusion assay that was also used to ensure the integrity of the plasma membrane. Cells were seeded on collagen-coated XF24 V7 plates (Seahorse Biosciences) at $4x10^4$ cells/well, allowed to attach for at least 2 hr, rinsed once and kept in 600 µl of sodium bicarbonate-free M199 medium supplemented with 1% BSA, 1 µM dexamethasone and 12 µM forskolin. After baseline measurements, additions were delivered in the following order in 75 µl injections through the instrument's individual injection ports; substrates (lactate/pyruvate or palmitate), ADP, and the mitochondrial ATP synthase inhibitor oligomycin. L-lactate (Sigma) and sodium pyruvate (Cellgro, Mediatech) were injected at 10 and 1 mM, respectively. Sodium palmitate (Sigma) was injected at 200 µM together with 10 mM L-malate (Sigma). When palmitate was tested, 0.5 mM carnitine (Sigma) was included in the incubation and equilibration medium to ensure mitochondrial transport of palmitate. Where indicated, the FAO inhibitor etomoxir (Sigma) was included in incubation and equilibration medium at 50 µM final concentration. After addition of the substrates, 5 mM ADP (Sigma) was injected to drive maximum respiration by mimicking a state of energy demand. Lastly, 1 µM oligomycin (Calbiochem) was injected to derive the portion of OCR used for ATP synthesis. In all experiments, parallel samples were run in the absence of any treatment to ensure stable baselines as a quality control parameter

for the bioenergetic health of the cells. OCR was measured at 37°C in 6 replicates in independent wells of the same plate. The number of independent experiments for each OCR measurement is indicated in figure legends.

Of note, ADP can be taken up by intact hepatocytes consistent with reports in several other cell types (Chaudry, 1982), and pilot studies confirmed comparable induction of ADP-driven OCR in hepatocytes can be achieved in the absence or presence of digitonin permeabilization (data not shown). For these reasons, intact hepatocytes were used in all OCR measurements. In addition, we measured intracellular ADP levels in hepatocytes after addition of 5 mM ADP to the medium and found this concentration to be 4.25 ± 0.10 mM under these conditions. OCR values in main Figures 3 and 4 represent the difference between the maximal rate in the presence of ADP and the rate after addition of oligomycin, thus indicating ATP production by mitochondrial oxidative phosphorylation. We also measured the oligomycin-inhibitable portion of OCR in the absence of ADP. Table S1 summarizes the OCR values in the absence and presence of ADP for all substrates and genotypes tested.

Analysis of mitochondria mass in primary hepatocytes. Primary *Bad* +/+ and -/- hepatocytes were seeded onto collagen-coated glass bottom culture dishes and cultured for 1 day. The cells were then incubated with 300 nM of MitoTracker Green (Invitrogen) for 30 min at 37°C, washed twice with HBSS, and visualized using a Leica DMI6000B microscope at a magnification of 63x. Fluorescence intensity was analyzed using the Leica Application Suite v3.5.0 and ImageJ v1.46r. All samples were processed in parallel and images captured in the same session using the same imaging parameters.

Microarray profiling and gene set enrichment analysis (GSEA). 1 µg of liver RNA was subjected to microarray analysis using the Affymetrix gene 1.0 ST mouse arrays containing transcripts of ~28,000 well-annotated genes. Affymetrix array hybridization and scanning was performed by the Microarray Core Facility of the Dana-Farber Cancer Institute. Expression values were normalized using the Robust Multichip Analysis (RMA) algorithm (Irizarry et al., 2003). Samples from *Bad* +/+ and -/- liver were compared using GSEA (Mootha et al., 2003; Subramanian et al., 2005). Curated gene sets (C2) and Gene Ontology based gene sets (C5) were used from the Molecular Signatures Database present at the GSEA website (http:// www.broad.mit.edu/gsea/). A custom gene-set corresponding to mitochondrial β-oxidation was also added to the analysis. Gene sets were permuted 1,000 times to determine false discovery rate (FDR) corrected p-values. Over-represented gene-sets were selected by applying nominal p-value cut-off of 0.05 and FDR of 0.25.

RNA preparation and quantitative real-time PCR. For real time PCR, RNA was prepared and analyzed as previously described (Danial et al., 2008). Primers for cyclophilin served as internal controls for the quality of RNA. The sequence of primers is available upon request.

Antibodies. The following antibodies were used for assessment of BAD phosphorylation and components of the insulin signaling pathway; total BAD (#9292), pS155 BAD (#9297), pS112 BAD (#5284), and pS136 BAD (#5286), total IR (#3025), pY1162 IR (#3024), total AKT (#9272), pS308 AKT (#9275), pS473 AKT (#9271), total GSK-3β (#9315), and pSer21/9 GSK-3 α/β (#9331) (Cell Signaling Technology). The anti-BAD antibody Ab 10929 was used for BAD immunoprecipitation (Yang et al., 1995). The anti-VDAC (anti-porin 31-HL) and anti-β-actin antibodies were purchased from Calbiochem and Sigma, respectively.

***In vivo* insulin signaling studies.** After an overnight fast, mice were injected intraperitoneally with saline or insulin (Humulin R) at 0.1 U/g of body weight and sacrificed by cervical dislocation 10 min post injection. The liver and gastrocnemius muscle were rapidly removed and frozen in liquid nitrogen. Tissue powders were generated using liquid nitrogen-cooled mortar and pestle and extracted in 0.5 ml of lysis buffer (20 mM Tris pH 7.4, 5 mM EDTA pH 8.0, 10 mM $Na_4P_2O_7$, 100 mM NaF, 2 mM Na_3Vo_4, 1% NP-40, 1 mM PMSF, 6 µg/ml Aprotinin, and 6 µg/ml Leupeptin) using Qiagen Tissue Lyser II. The samples were centrifuged at 14,000 RPM for 30 min at 4°C, and the supernatants were transferred to fresh tubes. IRS-1-associated PI3K activity was measured in IRS-1 immunoprecipitates as previously described (Lee et al., 2012). For analysis of distal insulin signaling components, 60 µg of protein was resolved on 4-12% gradient NuPAGE gels (Invitrogen) and analyzed by western blotting using the indicated antibodies.

Assessment of insulin signaling in primary hepatocytes. Primary hepatocytes were plated at $5.0x10^5$ cells/well in 6-well plates and serum starved for 14.5 hr in M199 media. They were subsequently treated with 100 nM insulin (Sigma-I6634) for 7 min, washed in PBS, and lysed in 100 µl of lysis buffer (20 mM Tris pH 7.4, 5 mM EDTA pH 8.0, 10 mM $Na_4P_2O_7$, 10 mM NaF, 2 mM Na_3Vo_4, 1% NP-40 1%, 1 mm PMSF, 6 µg/ml Aprotinin, 6 µg/ml Leupeptin), and 30 µg of protein lysate was fractionated on a 4-12% NuPAGE gel for western blot analysis using the indicated antibodies.

Assessment of BAD phosphorylation. Wild-type C57BL/6J mice were fasted overnight or refed for 6 hr after overnight fasting. Livers were excised and homogenized on ice in lysis buffer containing 10 mM Tris pH 7.0, 15 mM EDTA pH 8.0, 0.6 M sucrose, 15 mM β-mercaptoethanol, protease and phosphatase inhibitors (Roche). The homogenates were incubated on ice for 20 min and subsequently centrifuged at 14,000 rpm for 30 min at 4°C, and supernatant collected. 60 µg of protein was analyzed by western blotting using the indicated phospho-BAD or total BAD antibodies.

For assessment of BAD phosphorylation in *ob*/*ob* and *ob*/+ mice, livers were harvested from mice fasted for 24 hr or refed for 1 hr after fasting. Livers were homogenized on ice in a buffer containing 20 mM Tris-HCl pH 7.5, 137 mM NaCl, 10% glycerol, 2 mM EDTA pH 8.0, 2 mM Na_3Vo_4, protease inhibitors (Roche), and phosphatase inhibitors (PhosStop, Roche). The homogenates were incubated on ice for 20 min and then centrifuged at 14,000 rpm for 30 min at 4°C. The supernatant was collected with a gel-loading tip (to discard the top layer of fat) and transferred to a fresh tube. 60 µg of protein lysate was analyzed for total BAD protein levels by western blotting, and 2 mg of protein lysate was immunoprecipitated with an anti-BAD antibody [Ab 10929, (Yang et al., 1995)]. For immunoprecipitations, a final lysate volume of 500 µl per sample was incubated with 30 µl of protein A-conjugated sepharose CL-4B beads (GE Healthcare) for 30 min at 4°C with rotation. The pre-cleared lysates were transferred to a fresh tube and incubated with Ab 10929 at 1:500 dilution overnight at 4°C with rotation. Subsequently, 30 µl of protein A-conjugated sepharose beads were added and incubated for another 2 hr at 4°C with rotation. The beads were then washed 3 times with lysis buffer, resuspended in NuPAGE LDS sample buffer, heated for 5 min at 95°C, and loaded on a 4-12% NuPAGE gel for western blot analysis.

SUPPLEMENTAL REFERENCES

Bain, J.R., Schisler, J.C., Takeuchi, K., Newgard, C.B., and Becker, T.C. (2004). An adenovirus vector for efficient RNA interference-mediated suppression of target genes in insulinoma cells and pancreatic islets of langerhans. Diabetes 53, 2190-2194.

Chaudry, I.H. (1982). Does ATP cross the cell plasma membrane. Yale J Biol Med 55, 1-10.

Irizarry, R.A., Hobbs, B., Collin, F., Beazer-Barclay, Y.D., Antonellis, K.J., Scherf, U., and Speed, T.P. (2003). Exploration, normalization, and summaries of high density oligonucleotide array probe level data. Biostatistics 4, 249-264.

Lee, D.H., Huang, H., Choi, K., Mantzoros, C., and Kim, Y.B. (2012). Selective PPARgamma modulator INT131 normalizes insulin signaling defects and improves bone mass in diet-induced obese mice. Am J Physiol Endocrinol Metab 302, E552-560.

Matsumoto, M., Pocai, A., Rossetti, L., Depinho, R.A., and Accili, D. (2007). Impaired regulation of hepatic glucose production in mice lacking the forkhead transcription factor Foxo1 in liver. Cell Metab 6, 208-216.

Mootha, V.K., Lindgren, C.M., Eriksson, K.F., Subramanian, A., Sihag, S., Lehar, J., Puigserver, P., Carlsson, E., Ridderstrale, M., Laurila, E., Houstis, N., Daly, M.J., Patterson, N., Mesirov, J.P., Golub, T.R., Tamayo, P., Spiegelman, B., Lander, E.S., Hirschhorn, J.N., Altshuler, D., and Groop, L.C. (2003). PGC-1alpha-responsive genes involved in oxidative phosphorylation are coordinately downregulated in human diabetes. Nat Genet 34, 267-273.

Subramanian, A., Tamayo, P., Mootha, V.K., Mukherjee, S., Ebert, B.L., Gillette, M.A., Paulovich, A., Pomeroy, S.L., Golub, T.R., Lander, E.S., and Mesirov, J.P. (2005). Gene set enrichment analysis: a knowledge-based approach for interpreting genome-wide expression profiles. Proc Natl Acad Sci U S A 102, 15545-15550.

Wu, M., Neilson, A., Swift, A.L., Moran, R., Tamagnine, J., Parslow, D., Armistead, S., Lemire, K., Orrell, J., Teich, J., Chomicz, S., and Ferrick, D.A. (2007). Multiparameter metabolic analysis reveals a close link between attenuated mitochondrial bioenergetic function and enhanced glycolysis dependency in human tumor cells. Am J Physiol Cell Physiol 292, C125-136.

Yang, E., Zha, J., Jockel, J., Boise, L.H., Thompson, C.B., and Korsmeyer, S.J. (1995). Bad, a heterodimeric partner for Bcl-XL and Bcl-2, displaces Bax and promotes cell death. Cell 80, 285-291.

Yoon, J.C., Puigserver, P., Chen, G., Donovan, J., Wu, Z., Rhee, J., Adelmant, G., Stafford, J., Kahn, C.R., Granner, D.K., Newgard, C.B., and Spiegelman, B.M. (2001). Control of hepatic gluconeogenesis through the transcriptional coactivator PGC-1. Nature 413, 131-138.